Holocene lake-level changes in the Siljan Lake District – Towards validation of von Post's drainage scenario

Savvas Paradeisis-Stathis

Dissertations in Geology at Lund University,
Master's thesis, no 600
(45 hp/ECTS credits)

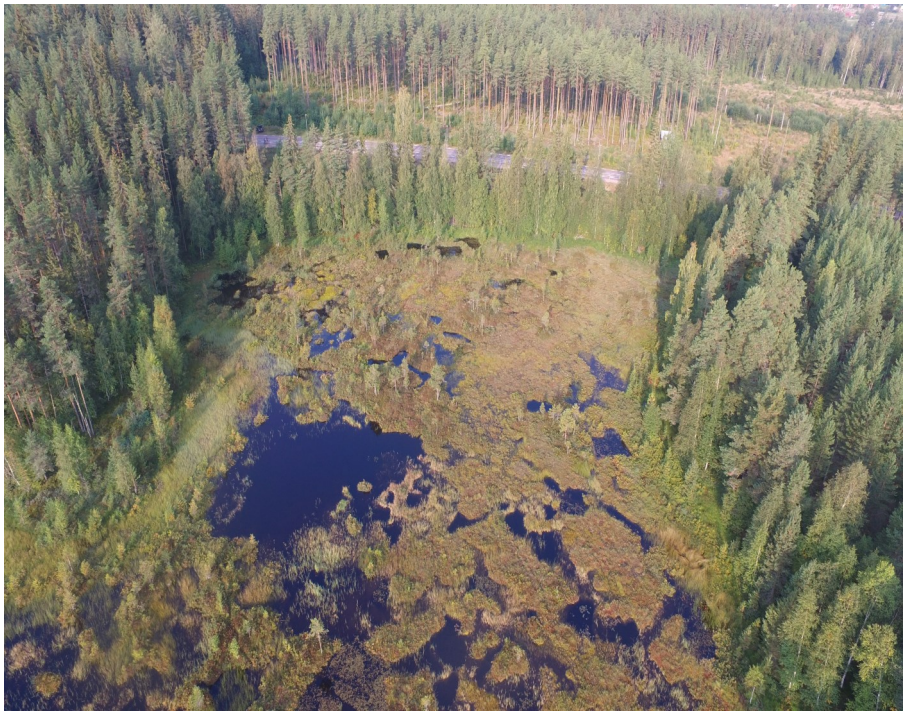

Department of Geology
Lund University
2020

Holocene lake-level changes in the Siljan Lake District – Towards validation of von Post's drainage scenario

Master's thesis
Savvas Paradeisis-Stathis

Department of Geology
Lund University
2020

Contents

Cover Picture: The peat bog in Heden. Distribution permit from LMV, LM2020/009398.

Holocene lake-level changes in the Siljan Lake District – Towards validation of von Post's drainage scenario

SAVVAS PARADEISIS-STATHIS

Paradeisis-Stathis, S., 2020: Holocene lake-level changes in the Siljan Lake District – Towards validation of von Post's drainage scenario. *Dissertations in Geology at Lund University*, No. 600, 36 pp. 45 hp (45 ECTS credits).

Abstract: The Dalarna province in south-central Sweden shows a great variety of geological evidence from the Late Quaternary. A peculiar deglaciation pattern, along with unique hydrological conditions, has left a lot of space for speculations over the palaeoenvironmental conditions during the early Holocene. Lake Siljan is in the southern perimeter of the Siljan impact structure, the most prominent in Europe. At deglaciation, c. 10.6 kyr ago, the retreating ice margin was followed by the inundation of the Ancylus Lake, forming the highest shoreline at c. 205 m a.s.l. in the eastern part of the Siljan basin. However, due to fast glacio-isostatic rise and consequent shore regression, the Siljan basin got isolated from the Baltic and formed the ´ancient Lake Siljan,´ probably as early as c. 10 kyr ago. In 1934, the Swedish geologist Lennart von Post published a fascinating study, proposing a scenario of catastrophic drainage of ancient Lake Siljan, at which the outflow through the Åkerö channel moved northwards, forming the present outlet of River Österdalälven at the town of Leksand. This drainage event led to a lake-level drop of about 6 m. At the same time, also according to von Post (1934), a basin at Heden, now a peat bog located 2 km south of Leksand, that before the drainage was part of Lake Siljan, became isolated. The present study is an evaluation of von Post's scenario by employing both traditional and modern geological techniques to sediment records from two coring locations, at Åkerö and Heden. The main findings suggest that during a stochastic high lake level stand, areas around the lake became submerged, and erosion processes were initiated that led to the opening of the new outlet at Leksand and the lake drained at some point close to 8.8 cal kyr BP. The aftermath of this drainage rerouting found the previous outlet channel at Åkerö abandoned, and the basin in Heden isolated. The drainage scenario, as suggested by von Post (1934), is thus confirmed but took place close to 2000 years earlier than was initially proposed, based on pollen zonation and before the development of accurate chronological dating techniques.

Keywords: Lake Siljan, Dalarna, basin isolation, catastrophic drainage, early Holocene, lake sediments, XRF scanning, C/N ratio, magnetic susceptibility, pollen, Ancylus Lake

Supervisor(s): Per Möller, Dan Hammarlund, and Karl Ljung

Subject: Quaternary Geology

Savvas Paradeisis-Stathis, Department of Geology, Lund University, Sölvegatan 12, SE-223 62 Lund, Sweden.
E-mail: sa7338-pa@student.lu.se

Holocena sjönivåförändringar i Siljan - Mot en validering av von Posts dräneringsscenario

SAVVAS PARADEISIS-STATHIS

Paradeisis-Stathis, S., 2020: Holocena sjönivåförändringar i Siljan - Mot en validering av von Posts dräneringsscenario. *Examensarbeten i geologi vid Lunds universitet*, Nr. 600, 36 sid. 45 hp.

Sammanfattning: Landskapet Dalarna i södra centrala Sverige uppvisar en stor variation av kvartärgeologiska sediment och landformer, bildade från deglaciationen i tidig Holocen och senare. Ett speciellt deglaciationsmönster, tillsammans med unika hydrologiska förhållanden, har lämnat utrymme för spekulationer över paleo-miljömässiga förhållandena under det tidiga Holocen. Siljanbassängen, belägen i det södra randområdet av Europas största impakt-stuktur började bli isfri för c. 10.6 tusen år sedan. Härvid följde Ancylussjön, ett av Baltiska sänkans havs/ sjöstadier, den tillbakasmältande isranden in i Siljanbassängen och utbildade i dennas sydöstra del en högsta kustlinje på c. 205 m.ö.h. Emellertid, på grund av glaci-isostatisk grundad, snabb landhöjning och därmed orsakad strandlinjeförskjutning, kom Siljanbasängen att tidigt bli isolerad från Ancylussjön, troligen redan för 10 tusen år sedan, varvid ´Siljanfornsjön´ bildades. 1934 publicerade den svenska geologen Lennart von Post ett fascinerande scenario som föreslog att Siljanfornsjön, med en högre vattennivå än nuvarande Siljan, erfor en katastrofal, snabb dränering, vid vilken det dåvarande utflödet genom Åkerökanalen förflyttade sig norrut och utbildade det nuvarande utloppet för Österdalälven vid Leksand. Denna dräneringshändelse ledde till att Siljan sänktes c. 6 meter. Samtidigt, också enligt von Post (1934), isolerades en bassäng vid Heden, idag en torvmosse belägen c. 2 km söder Leksand, men vid dräneringstillfället en vik av Siljanbassängen. Föreliggande studie är en utvärdering av von Post's dränerings-scenario, genomfört genom att använda traditionella kvartärgeologisk undersökningsmetoder, men framför allt genom att använda modern dateringsmetodik, på två sedimentkärnor uppborrade på samma platser som von Post´s lokaler vid Åkerö och Heden. De viktigaste resultaten indikerar att ett onormalt högvattenstånd i Siljan för c. 8.8 tusen år sedan gjorde att sjön fann ett nytt utloppsområde och att snabba erosionsprocesser skapade ett utlopp med en lägre pasströskel än för det tidigare Åkerö-utloppet. Följden blev att den tidigare Åkerökanalen torrlades och att sjöbassängen vid Heden isolerades från Siljan. Det dränerings-scenario som föreslogs av von Post (1934) har i föreliggande studie mer eller mindre bekräftats, men dräneringshändelsen ägde rum bortåt 2000 år tidigare än vad som föreslogs av von Post baserat på pollenzonering och en kronologi pre-14C.

Nyckelord: Siljan, Dalarna, sjöisolering, katastrofal dränering, tidig Holocen, sjösediment, XRF-skanning, C/N-kvot, magnetisk susceptibilitet, pollen, Ancylussjön

Handledare: Per Möller, Dan Hammarlund, and Karl Ljung

Ämnesinriktning: Kvartärgeologi

Savvas Paradeisis-Stathis, Geologiska institutionen, Lunds Universitet, Sölvegatan 12, 223 62 Lund, Sverige.
E-post: sa7338-pa@student.lu.se

1 Introduction

The origin and formation of lake basins are sometimes subject to drastic geological events and constant forces of alteration (Håkanson and Jansson 1983). Tectonism, volcanism, meteorite impacts, and glacial activity, in combination with weathering, erosion, transport, and deposition processes, have, to a great extent, formed the lacustrine landscapes of our time. Solely glacial activity during the last glacial period developed a vast number of small lakes that nowadays almost dominate in the Nordic landscape, which are of significant palaeoenvironmental importance (Håkanson and Jansson 1983). More specifically, lake sediments are considered as central areas of investigation for understanding the patterns of deglaciation (Calles 1985) and later palaeoenvironmental change.

The study area of this thesis is the southeastern part of Lake Siljan, situated in the province of Dalarna in central Sweden (Fig. 1). Lake Siljan is located in the southern perimeter of the Siljan impact structure (Fig. 1A), a circular formation close to 50 km in diameter that resulted from a meteorite impact during the Devonian period (380 Ma BP) (Holm-Alwmark et al. 2017). The Siljan impact structure is the largest known in Europe. At the center of the impact is a dome (32 km in diameter and reaching more than 500 m a.s.l.) composed of granite from the Precambrian time (Smith and Peterson 2014). The central dome is flanked by down-faulted and imbricated Silurian and Ordovician sedimentary rocks and a depression that hosts a lake system with Lake Oresjön and Lake Skattungen in the north, draining into Lake Orsasjön in the NW, continuing into Lake Siljan in the south, which eventually is drained by River Österdalälven with an outlet in the SE at Leksand. The unconsolidated sediments in the area of investigation are primarily of glacial and postglacial origin (Fig. 1A).

The Late Weichselian glaciation left a landscape with tracts of drumlins indicating a deglacial ice flow from NNW. The Siljan lake basin started to become deglaciated at around 10,600 cal yr BP (Stroeven et al. 2016) and soon after was gradually inundated by the Ancuylus Lake (von Post 1934) (Fig. 1B). Field observations suggest that the highest shoreline formed at 205 m a.s.l. in the SE, while, due to the differential isostatic uplift, it was formed at c. 210 m a.s.l. in the north (Nordell 1984), although reconnaissance based on the digital elevation model (DEM) revealed that more elevated shorelines occur at c. 220 m a.s.l. north of Lake Orsasjön (Per Möller, personal communication 2020). Isostatic uplift of the area resulted in shoreline regression of the Ancylus Lake, as evidenced from beach ridges, at gradually lower altitudes below the highest shoreline; eventually the Orsasjön-Siljan basin became isolated from the Ancylus Lake at which it had a lake level of approximately 168.5 m a.s.l. in the threshold area in the SE (Leksand), while the contemporary shoreline in the north (Lake Orsasjön) is now located at around 180 m a.s.l. due to differential uplift (von Post 1934). Today, the shoreline of the lake system is at approximately 162 m a.s.l., thus exhibiting an apparent difference of 6.5 m in the outlet area of River Österdalälven in comparison with the lake level after the isolation from the Ancylus Lake.

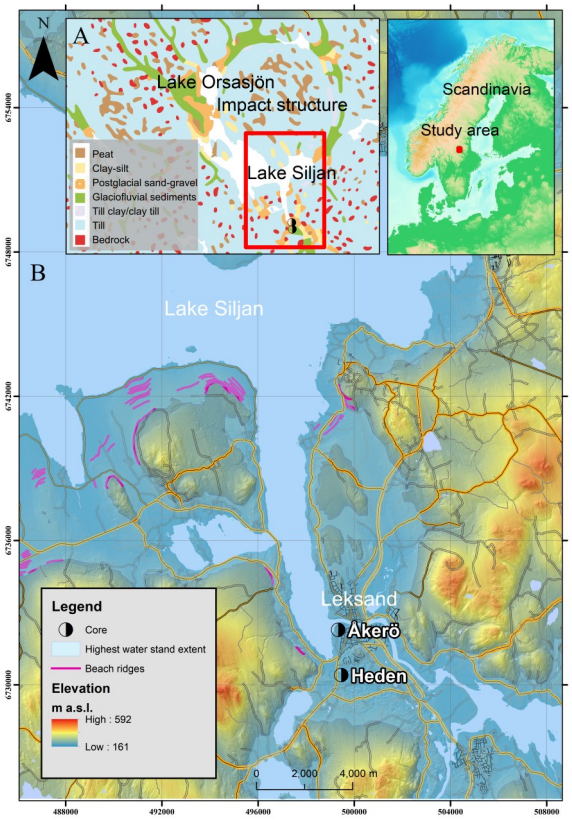

Fig. 1. Location map. A. The broader area around the Siljan ring, the major lakes, and Quaternary deposits. Till dominates at the surface, but eskers and other glaciofluvial deposits occur, predominantly in low-lying areas. The red frame indicates the location of frame B. Data source: Geological Survey of Sweden (SGU kartvisare, sgu.se). B. Elevation map and coring locations. Areas below 205 m a.s.l. (the local altitude of the deglacial highest shoreline formed by the Ancylus Lake) are marked in transparent bluish. Purple lines indicate the position of identified relict beach ridges. Data source: Lantmäteriet (lantmateriet.se)

Based on topographic and stratigraphic observations, von Post (1934) formulated the hypothesis that there was a somewhat catastrophic drainage of Lake Siljan in the Leksand area at which the lake found a new outlet, leading to a lowering from 168.5 m to the present lake level of c. 162 m a.s.l. The lake-level lowering led to the abandonment of the Åkerö channel (Fig. 2), According to von Post (1934), this was triggered by an exceptionally high lake level event reaching a slightly higher depression north of the Åkerö channel (Fig. 3). Rapid erosion into the sandy-silty sediments led to greater depths than that of the Åkerö channel, which got abandoned, and the Siljan lake basin was lowered to its present position. Furthermore, areas above 162 m were cut off from the lake and gradually dried-up. According to von Post (1934), stratigraphic evidence of this drainage and lake level lowering, leading to isolation of basins at altitudes between 168.5 and 162 m a.s.l., is recorded by a transition from mica-rich gyttja to lake mud at Heden, presently a peat bog, situated 2 km south of Åkerö (Fig. 2).

This study aims to identify and describe the sedimentary layers that reflect the period before and

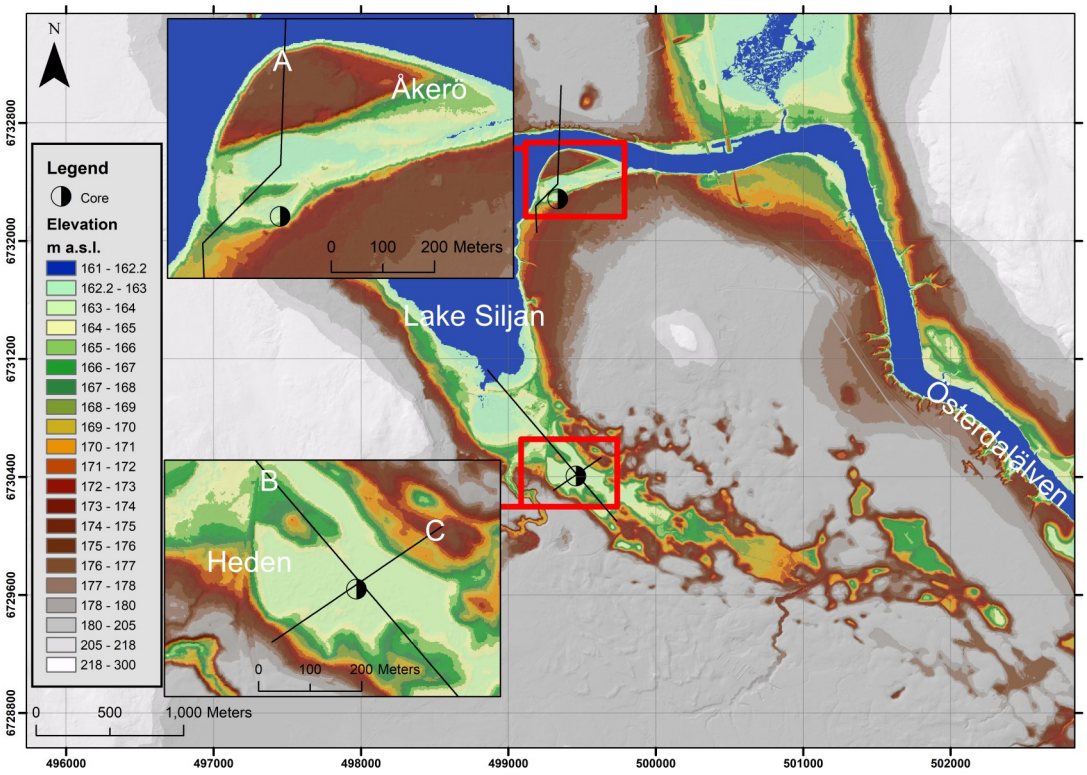

Fig. 2. Classified elevation map with hill-shade effect from a digital elevation model (DEM) of the southern part of Lake Siljan and its outlet, River Österdalälven. The classification permits a better understanding of the topographic relief. The boxes focus on the vicinity of the coring sites Åkerö and Heden. Black lines show the location of the cross profiles, as presented in Figs 3, 4, and 5. Data source: Lantmäteriet (lantmateriet.se)

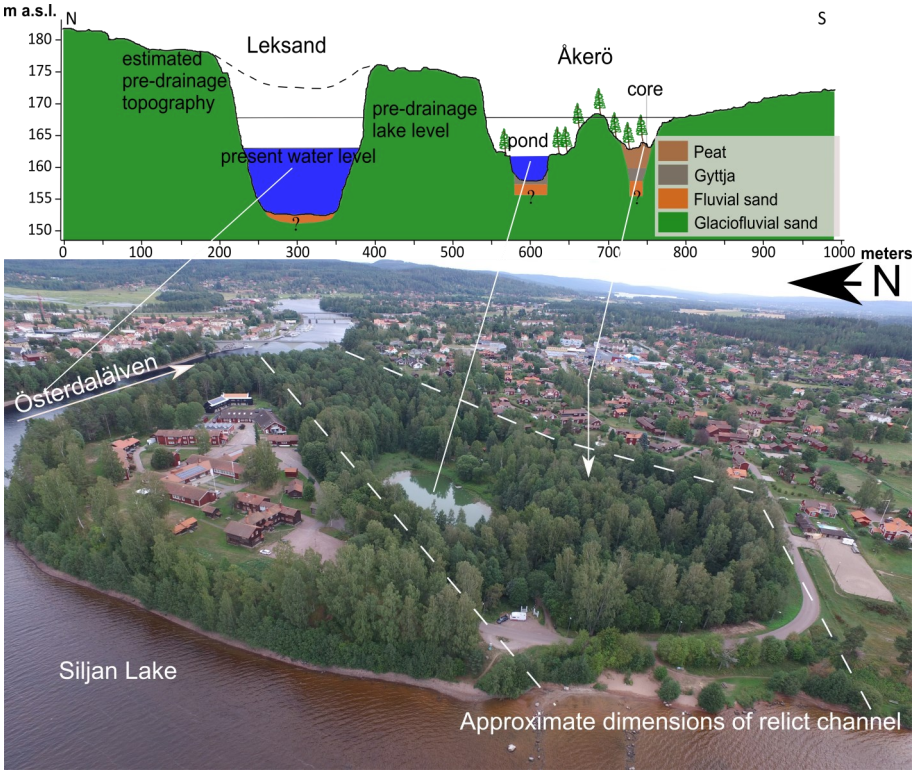

Fig. 3. Cross profile (A in Fig. 2) over the past and present outlet of Lake Siljan. The topography profile is a product of a DEM with 3D Analyst in ArcGIS. The exact boundary between fluvial sand and glaciofluvial sand has not been surveyed in the present study and is marked with a question mark. Drone image of the Åkerö site. The dashed line indicates the approximate position of the relict drainage channel. The coring site is close to the southern side of the relict channel. Distribution permit from LMV, LM2020/009398.

after this postulated drainage event or ideally the drainage event itself and provide accurate dating of when the incident happened. Based on pollen data, von Post (1934) argued that the drainage event occurred during the Littorina maximum in the mid-Holocene. According to evidence from the SE Baltic coast of Sweden, the Littorina maximum started with a rapid sea-level rise around 7.6 cal kyr BP due to the decay of the Laurentide Ice Sheet and culminated at 6.5 cal kyr BP due to the complete melting of the Ice Sheet section in North America (Yu et al. 2007). By identifying and dating the event, it will be possible to evaluate the drainage scenario of von Post (1934) regarding both its magnitude and its timing, by employing both traditional and modern geological techniques.

2 Site description, materials, and methods

The following section will describe the motivation of coring sites and the steps that were followed for sediment extraction, sub-sampling, and data acquisition and processing. The employed methods and techniques were sediment description, magnetic susceptibility measurements, XRF scanning, and multivariate statistics of elemental data, *Carbon* and *Nitrogen* analysis, pollen analysis, radiocarbon dating, and evaluation of digital elevation models.

2.1 Site description

The catastrophic drainage scenario (von Post 1934) described in the introduction is mainly based on interpretations of sediments from two localities close to Leksand, the Heden and Åkerö sites that are re-investigated and re-evaluated in this thesis.

The Heden site (60°42'33.4" N, 14°59'24.3" E) is an infilled former lake basin with gyttja overlain by peat. The peat bog surface is approximately at 163 m a.s.l. (Fig. 2) and is connected to a small stream. The peat bog surface has numerous water-filled depressions, probably due to modern peat extraction, that make the crossing of the bog a challenge. The depression is surrounded by silty-sandy deposits with a hummocky topography, reaching altitudes higher than 170 m a.s.l. As this is well below the highest shoreline at c. 205 m a.s.l., these sediments most probably represent glaciofluvial subaqueous fan deposits. The cored gyttja-peat succession, with sand at the bottom, was 8.25 m.

The Åkerö site (60°43'34.1" N 14°59'16.1" E) marks the by von Post (1934) postulated former drainage outlet of Lake Siljan, cut down into glaciofluvial sand with up to 15 m high, steep, channel walls. The present bottom of the channel at approximately 163 m a.s.l., (Fig. 2) is not the erosional bottom of the channel. As indicated in the cross profile in Fig. 3, there are two basins, of which a pond still occupies the northern part of the palaeochannel. In contrast, the southern basin in the channel has an infill succession of gyttja and peat on top of fluvial sand, the latter marking the stream bed of the Dalälven River before the drainage event. In between is an erosional remnant from the time when the water flowed through the channel. The length of the cored sequence at Åkerö is 6.75 m.

The DEM suggests that both localities where once part of a larger ancient Lake Siljan. Heden is in a fjord-like basin and Åkerö in a channel-like depression that connects to the present River Österdalälven (Fig. 2). According to the scenario under investigation, the ancient Lake Siljan can be defined as the lake stage of the current Lake Siljan, when lake-waters were covering a greater area than today and included the Heden basin. Moreover, the drainage of the lake waters at that stage was taking place through Åkerö, a slightly shallower channel than the current one at Leksand.

2.2 Sediment extraction

The retrieved cores at Heden and Åkerö were taken with a Russian peat sampler with 7.5 cm or 5 cm diameters. Coring was done in two nearby holes in which 1 m sediment core lengths were alternatively retrieved at gradually increasing sediment depths, and mostly with an overlap of 20 cm between the cores. The cores were described and photographed in the field, then placed in supportive liners and wrapped in plastic film before being transported and stored in the cold room at the Department of Geology at Lund University. A more thorough description of the sediments was later carried out in the laboratory before sub-sampling.

2.3 Magnetic susceptibility

Magnetic susceptibility of lacustrine sediments measures the degree of potential magnetisation of detrital minerogenic material. It is a method applied for core correlation and for inferring specific information on the chemical and biological composition of the sediments (Thompson et al. 1975). The measurements were carried out at the Palaeomagnetic laboratory at the Department of Geology, which is equipped with an automated platform and a Bartington MS2 Instrument. The data were acquired at 4 mm steps and were registered in SI units with the 0.1 range where the average of several readings over 10 s is recorded. Every magnetic measurement was later normalized with the magnetic signal of the air in the laboratory through a typical procedure. In other words, every data point on the core was normalized by subtracting the average of two measurements, at the same and an earlier depth, in the air.

2.4 XRF scanning

The XRF technique involves the bombardment of the surface of the sediment core with high-energy electrons that excites the elements in the sediments and emit their unique signatures. In this way, it is possible to detect relative variations in the elemental concentrations of the sedimentary sequence (Rothwell and Croudace 2015a). The instrument that was used for the analysis was a stationary Itrax Core Scanner at the facilities of the Center for Geo Genetics at the Globe Institute, Copenhagen University, Denmark. The instrument is also designed to gather high resolution optical and radiographic images.

The XRF analysis of the sequences from the Heden and Åkerö sites was carried out on the lower sediment successions of the cores (sand and gyttja) up

to the transition to peat. The surface of every core exposed to the sensors of the XRF instrument was scraped perpendicularly to smooth uneven surfaces and to avoid contamination of the data. Hence, it was possible to minimize the loss of data due to blind spots placed on steep surfaces of the cores, which also cause lifting and lowering movements of the detector (Löwemark et al. 2019). However, small height variations could be analysed with good results (Cox Analytical Systems, 2019).

A high-resolution optical image that, among other applications, adjusts the distance and movement of the detector over the sediments was taken. In order to avoid drying up, cracking, and shrinking of the core from the long scanning hours, an XRF film (ultra-thin PET) was placed on the surface of the core. The film was carefully set to stick on the surface to avoid openings where water layers can form as they affect the signatures of the elements (Löwemark et al. 2019).

The electrons were delivered by an Rh tube, which is usually applied for identifying heavy elements (Cox Analytical Systems, 2019). The radiographic parameters were set to a voltage of 60 kV, current of 30 mA, exposure time of 1000 ms, and step size of 200 μm. The XRF parameters were set to a voltage of 30 kV, current of 50 mA, exposure time of 30 s, and step size of 1000 μm. Cores 9 and 11 from Heden were analysed with 7 s exposure time, and at 200 μm steps for higher depth resolution and because these cores showed richer transitions in the lithology. Post-processing of the XRF data took place in the Q-spec software. The program can normalize the results by the amount of the emitted coherent Rh electrons and correct for measuring errors by considering the counts per second of the different elements, the exposure time, and the typical elemental spectrum. In unpolluted clayey sediments, the Rh tube can typically detect Al, Si, S, Cl, K, Ca, Ti, Cr, Mn, Fe, Ni, Cu, Zn, Br, Rb, Sr, Zr, Mo, Ba, and Pb (Cox Analytical Systems, 2019). In this case, the recorded elements were Al, Si, P, S, Ar, K, Ca, Ti, V, Cr, Mn, Fe, Ni, Cu, Zn, Br, Ge, As, Rb, Sr, Y, Zr, Mo, La, Ce, Nd, Tm, and Yb. The elements Mg, Cl, Se, and Nb, were occasionally also captured, but overall, the data contained many empty cells and thus were excluded.

Two elemental ratios, Ca/Ti and Mn/Fe that are proxies for water level changes (Haberzettl et al. 2007; Jouve et al. 2013) and ventilation in the water column (Melles et al. 2012) respectively are also employed. The association of Ti to detrital runoff due to variations in the hydrological conditions (Haberzettl et al. 2007) and the positive and negative association of Ca to algae productivity (Olsen et al. 2013) and terrigenous material (Rothwell and Croudace 2015b) respectively, indicate that a high Ca/Ti reflect dry conditions and low lake stands while a low Ca/Ti reflect moister conditions and high stands (Haberzettl et al. 2007; Jouve et al. 2013). The association of high solubility of Mn to reduction conditions and the association of high solubility of Fe to oxidation conditions reflect redox conditions (Unkel et al. 2008) and in combination with the colour of the sediments and MS can indicate the oxygen levels and ventilation in the water column (Melles et al. 2012). Hence, a high Mn/Fe ratio reflects good ventilation and well-oxygenated waters.

2.5 Radiocarbon dating

Radiocarbon dating is a widely used technique to determine the age of organic inclusions in sedimentary successions. However, accurate dating of lacustrine environments may be problematic due to a lower $^{14}C/^{12}C$ ratio than in the atmosphere and because gyttja is vulnerable to contamination due to a sometimes small percentage of organic carbon (Lowe and Walker 2014). Sub-samples were taken in 2 cm thick slices, and they were representative of the major lithological units up to the transition from gyttja to peat sediments at the Heden and Åkerö sites. After wet-sieving, sampled material bigger than 0.02 mm, were set under a stereo microscope for collecting macrofossils (seeds, leaf fragments, bark, small twigs). The thickness of the sub-samples was varying down-core depending on the amount of available material.

A total of 13 AMS ^{14}C ages were determined at the AMS Radiocarbon Dating Laboratory, Department of Geology at Lund University, Sweden. The retrieved ages are presented as conventional radiocarbon years (conv. ^{14}C age) with one standard age deviation (1 σ; 68.2%), as well as calibrated calendar years (cal yr BP), calculated with the software package Oxcal 4.3.2 (Ramsey 2017) using IntCal 13 (mean age ±2σ; 95.4%).

2.6 Carbon and Nitrogen analysis

The C/N ratio based on elemental analysis of total organic C and N contents is a proxy for determining the palaeo-productivity and the origin of organic matter in lake sediments (Liiv et al. 2019). A low C/N ratio between 4-10 is indicative of high N content and a high proportion of aquatic organic matter while a high C/N ratio, especially above 20 is indicative of high C content and terrestrial organic matter (Meyers and Ishiwatari 1993; Liiv et al. 2019). The method was applied only to the record from Heden. A total of 50 sub-samples with approximately 0.5 cm^3 material was collected at regular intervals from cores 9 to 11, the three lowermost cores of Heden. The sub-samples were set in crucibles and the oven at 55 ^{o}C for a day. The material was then ground and stored in plastic vails. For sample preparation, the capsule method was employed, which is described in detail by Brodie et al. (2011). Furthermore, based on the scatter-plot test of the total organic carbon and total nitrogen, and the linear regression between the two, the presence of inorganic N was evaluated (Talbot 2001). The C/N ratios are reported after conversion to atomic ratios by multiplying with 1.167. The analysis was carried out at Lund University, using a Costech ECS 4010 elemental analyser.

2.7 Pollen analysis

It was not a primary aim of this study to perform a

holistic palaeoenvironmental reconstruction of Lake Siljan and its surroundings. However, it was found necessary to make a selective pollen analysis of sub-samples located close to the levels of radiocarbon dates within the Heden sediment core. In this way, it would be possible to triangulate with the pollen records from a nearby site and provide an indirect dating control. A total of five pollen samples of 1 cm^3 each were collected from core 10 at proximate depths to the radiocarbon samples. The pollen sample preparation followed an adapted procedure developed by the Danish palaeoecologist Johanes Iversen, as presented in Faegri et al. (1989). Lycopodium tablets were added to every sample. More than 500 pollen grains were identified in each sample under a light microscope. The pollen counts were converted to percentages in Tilia v.2.1.1. but the small number of sub-samples would not allow for the creation of a meaningful pollen diagram.

2.8 Maps and figures

Figures of magnetic susceptibility, XRF, and C/N ratios were produced in Matlab v. R2019a. Maps were produced in ArcMap v. 10.7.1, and data sources were Lantmäteriet (lantmateriet.se) and the Geological Survey of Sweden (SGU, sgu.se). The age-depth models were constructed using the code of Clam v. 2.3.2 (Blaauw 2010) in software R v. 3.6.3. The settings in Clam were smooth spline curve type, with 0.3 smoothing and calibration curves for terrestrial samples from the Northern Hemisphere (Reimer et al. 2013). For the use of Clam in R, the instructions and methodology by Flantua et al. (2016) were followed. Multivariate statistics were run in IBM SPSS v. 26. Maps and figures were edited in Inkscape v. 0.92.

3 Results and interpretations

3.1 Sediment descriptions

Heden: - The Heden site is a basin surrounded by glaciolacustrine sandy-silty sediments (Fig. 4), which at the coring site is infilled with approximately 8.15 m of gyttja and peat. To the NE of the basin, there is a low-elevated channel that hosts a stream (Fig. 5). Otherwise, the basin is bay-shaped and is surrounded by higher ground where some elevation intervals are exceptionally steep (Fig. 2). At the very bottom of the core (Table 1), a sandy sequence (unit 1) is succeeded by gyttja, which in the lower part is black, flaky, and smelly (unit 2A). It abruptly becomes lighter in colour at 814 cm (ebony-black) with darker laminations that, after extraction, turned from black to red (unit 2B). After that, at 807 cm, the gyttja becomes a lighter shade of black/dark brown (unit 2C) and then at 790 cm, turns back to a darker shade of black (unit 2D). After 730 cm (unit 2E), there is a textural change from firm to a "jelly" structure, and there are silty lenses. Another significant shift in the gyttja occurs at 560 cm

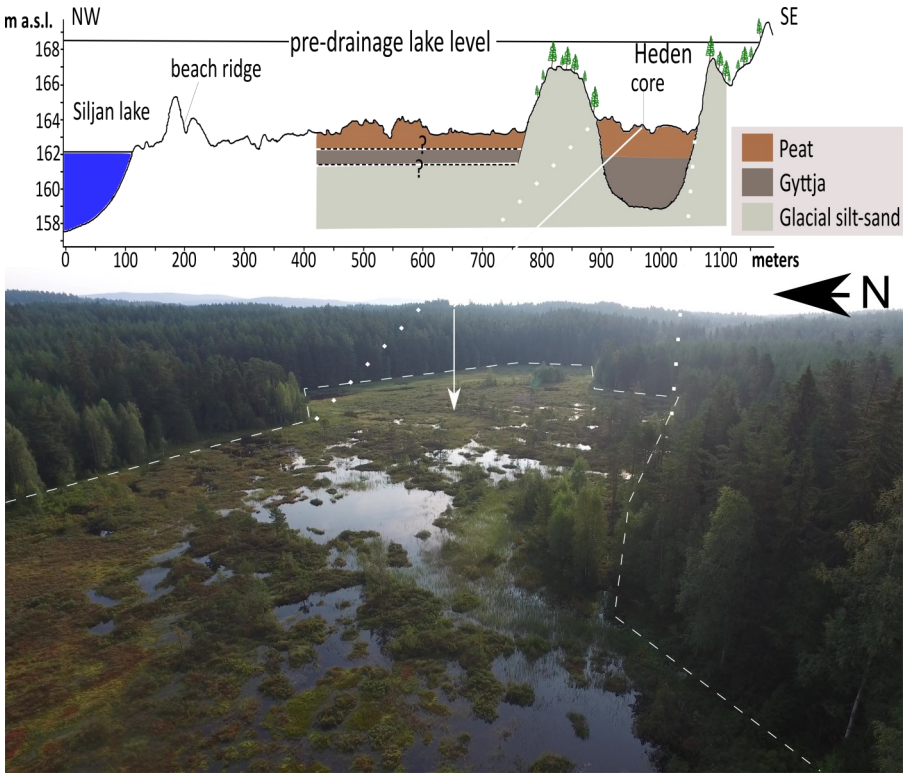

Fig. 4. Cross profile (B in Fig. 2) from Lake Siljan across the Heden basin. The topography profile is a product of a DEM with 3D Analyst in ArcGIS. The exact boundaries between peat, gyttja, and glacial silt-sand may differ away from the basin at Heden and are marked with question marks. Drone image of the Heden site. The dashed line marks the approximate area of the bog. The coring site is located close to the eastern center of the bog. Distribution permit from LMV, LM2020/009398.

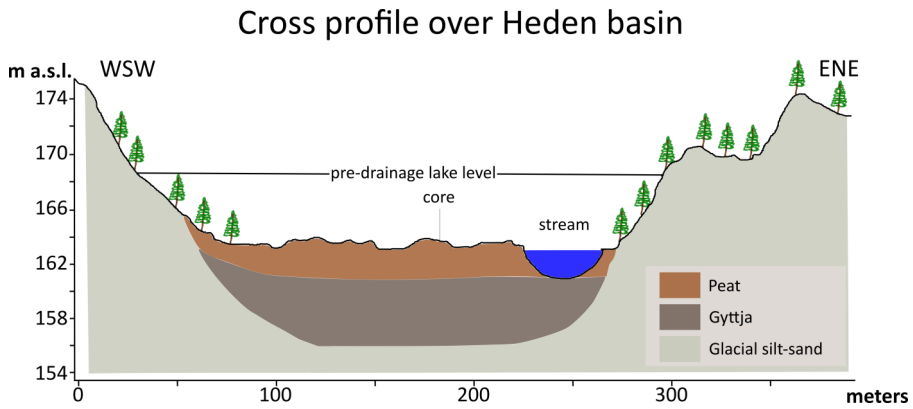

Fig. 5. Cross profile (C in Fig. 2) over the Heden basin. The topography profile is a product of a DEM with 3D Analyst in ArcGIS.

Table 1. Lithostratigraphic units identified in the Heden sediment record.

Depth (cm)	Unit	Lithology	Comments
0 – 32	3C	fresh sphagnum peat	
32 – 240	3B	sphagnum peat	sharp boundary to the upper unit, from 140 – 260 cm appearance of fen peat
240 – 328	3A	fen peat	gradual transition to the upper unit
328 – 390	2G	coarse detritus gyttja	gradual transition to the upper unit
390 – 560	2F	fine detritus gyttja	gradual transition to the upper unit, mixed with algae-rich gyttja towards the bottom
560 – 730	2E	algae-rich gyttja	gradual transition to the upper unit, oil black, silty lenses towards the bottom
730 – 790	2D	clay gyttja	gradual transition to the upper unit
790 – 807	2C	gyttja clay	sharp boundary to the upper unit, light black/dark brown
807 – 814	2B	gyttja clay	sharp boundary to the upper unit, ebony black, laminations that oxidized and turned red
814 – 818	2A	gyttja	sharp boundary to the upper unit, black, flaky, and smelly
818 – 825	1	sand	sharp boundary to the upper unit, sand continues for at least 15 cm more

(unit 2F) when it turns back to a lighter colour (dark brown); it acquires a firmer structure, and progressively becomes more abundant in organic material, and coarsens upwards (unit 2G). At the top of the sequence, the basin is infilled with minerotrophic fen peat (unit 3A) and then with ombrotrophic sphagnum peat (unit 3B). A more detailed description of the different sedimentological units and an optical image of the bottommost core are presented in Fig. 6 and 7 and for the sediments up to the beginning of peat in Appendix 1-5.

Heden, interpretation: - The sandy layer (unit 1) at the bottom should not be related to fluvial processes alone, because the Heden basin is only open to the NW while to the SE, the basin is closed. Moreover, the outlet of Lake Siljan at Åkerö was 2 km to the north of the Heden basin. Hence, water-flow at Heden must had been weak. The above suggests that the silty-sandy bottom sediments at Heden must have been deposited during deglaciation and most likely be glaciofluvial in origin, as is also marked by SGU (Fig. 1A). At the beginning of the gyttja sequence (unit 2A), the colour, the texture, and the smell of the sediments indicate high organic matter content. In unit 2B, there is an abrupt reduction in organic material, gyttja becomes richer in minerogenic content and interbeds laminae that became oxidized after exposure to the air. The brightness of the sediments often reflects the minerogenic content of gyttja. However, the exact type of gyttja is difficult to determine solely from variations in colour, and more accurate characterizations were also based on the C and N measurements (Fig. 6 and 7). Thereby, units 2B and 2C with respectively ebony black and light black/dark brown colour, have a change in the content of minerogenic or organic matter in the gyttja. Gyttja clay becomes clay gyttja in unit 2D after a darkening in the sedimentary record. The change in the texture and the darkening of the colour to oil black in unit 2E signal the transition to algae-rich gyttja. Unit 2E progressively becomes more abundant in organic material (fine detritus gyttja, 2F), which finally becomes coarser (coarse detritus gyttja, 2G). In the end, the lake became shallow, and peat started to grow and accumulate in areas with dense sedge vegetation.

Åkerö: - The Åkerö site is a depression that has

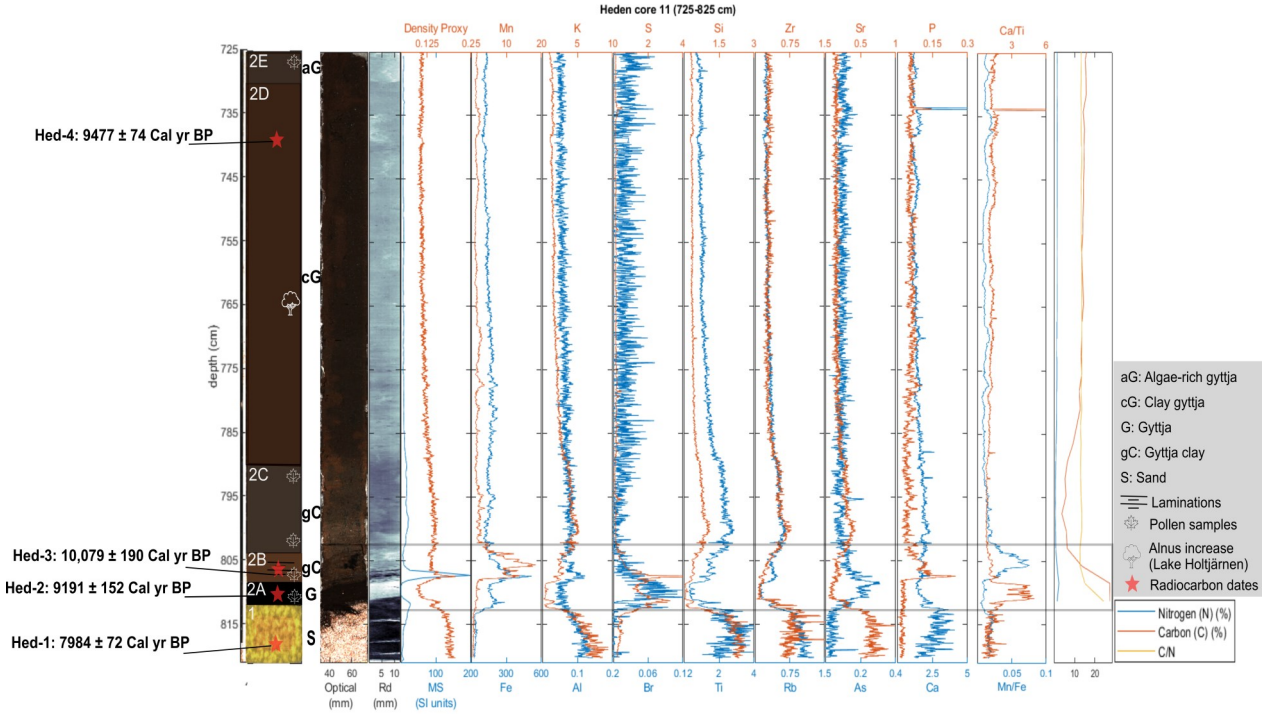

Fig. 6. Overview of core 11 (725 – 825 cm) from the Heden sediment record. From left to right, the log of lithology with assigned units, radiocarbon, and pollen samples. The optical and radiographic (RD) image, density, magnetic susceptibility (MS), relative concentrations of typical elements for lake surveying, Ca/Ti and Mn/Fe proxies, C and N contents, and C/N ratios. The box indicates an area of exceptional signal, areas where there is an evident short-term and compact change in most proxies. The length of the core is slightly off compared to the unit classification in Table 1 due to shrinking.

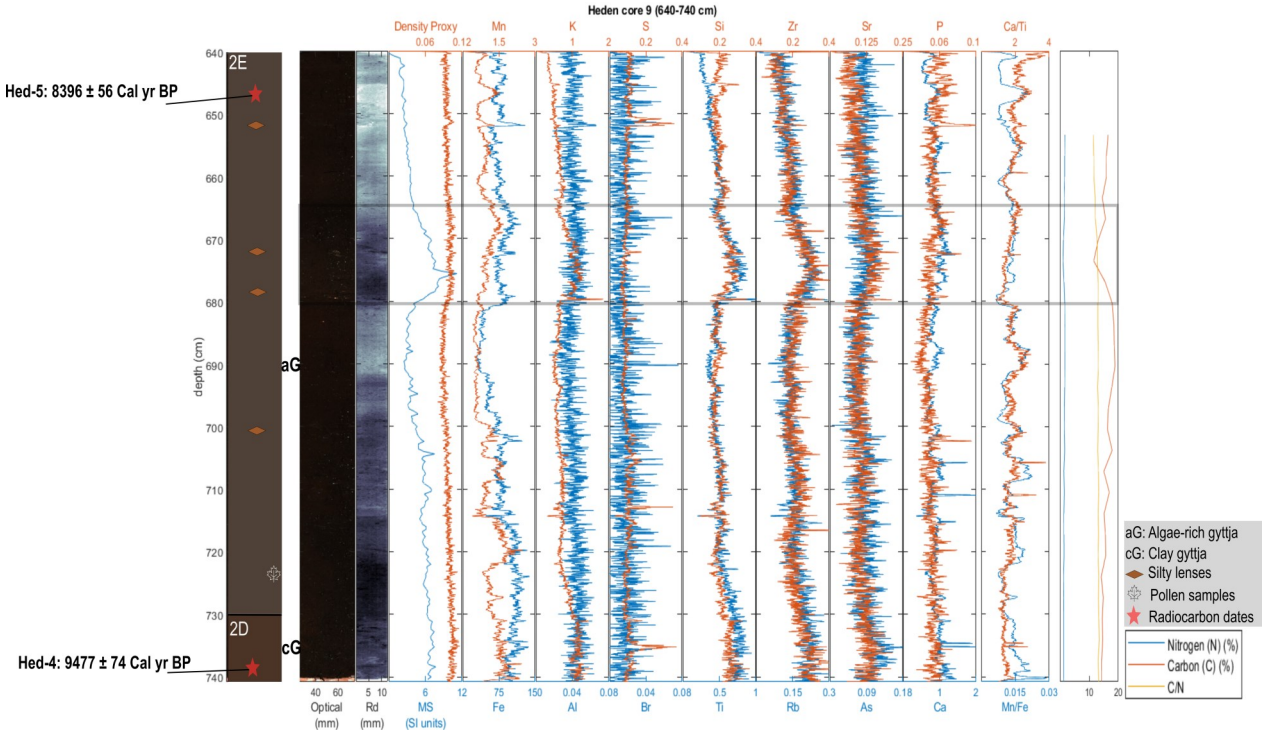

Fig. 7. Overview of core 9 (640 – 740 cm) from the Heden sediment record. From left to right, the log of lithology with assigned units, and radiocarbon samples. The optical and radiographic (RD) image, density, magnetic susceptibility (MS), relative concentrations of typical elements for lake surveying, Ca/Ti and Mn/Fe proxies, C and N contents, and C/N ratios. The box indicates a zone with an unusual signal.

topographical characteristics of a relict drainage channel, trending WSW-ENE (Fig. 2). The channel bottom hosts a number of partly sediment infilled basins along its present bottom, at c. 163 m a.s.l. The cored basin in

the WSW part of the Åkerö channel, close to its southern channel side, reveals a 6.75 m thick sediment succession of fluvial sand, gyttja, and peat (Fig. 3). The sedimentary sequence starts with a unit of fine sand (unit 1A) with layers of clayey silt (Table 2), followed by an erosional boundary towards medium sand (unit 1B). Unit 1 is in total 96 cm. Unit 2, 191 cm thick, is divided into four subunits, A-D. The sediment succession starts with silty/sandy gyttja (2A), followed by clay gyttja and fine and coarse detritus gyttja. At the gyttja stages, there are scattered silty/sandy lenses and occasionally sharp transitions to thick bands of inwashed minerogenic material (units 2B-2D). However, the gyttja becomes more organic-rich upwards, and is overlain by fen peat at a depth of 388 cm (unit 3), which is rich in wood remains in its upper part. A more detailed description of the different sedimentological units and an optical image of the bottommost sequence are presented in Fig. 8 and for the sediments up to the beginning of peat in Appendix 6-8.

Åkerö, interpretation: - The sandy units (1A and 1B) represent a stage when the channel was still active as the outlet of the Siljan lake basin. The clayey interbeds within unit 1A, and the shift to medium sand (unit 1B) indicate a change in the energy regime of the system. Clayey sediments typically get deposited during weaker river flows when the water is unable to carry and mobilize coarser sediments from the lake

Table 2. Lithostratigraphic units identified in the Åkerö sediment record.

Depth (cm)	Unit	Lithology	Comments
0 – 3	3E	forest peat	
3 – 170	3D	fen peat	sharp boundary to the upper unit, mix with sphagnum peat at the bottom
170 – 230	3C	sphagnum/fen peat	gradual transition to the upper unit
230 – 344	3B	fen peat	gradual transition to the upper unit, occasional bands with sphagnum peat
344 – 388	3A	moss peat	sharp boundary to the upper unit
388 – 400	2D	coarse detritus gyttja	gradual transition to upper unit, silty/sandy lenses
400 – 490	2C	fine detritus gyttja	sharp boundary to the upper unit, thick interbeds with higher minerogenic content
490 – 565	2B	clay gyttja	gradual transition to the upper unit
565 – 579	2A	silty-sandy gyttja	gradual transition to the upper unit, silty/sandy lenses towards the bottom
579 – 586	1B	medium sand	gradual/erosional transition to the upper unit
586 – 675	1A	fine sand	sharp boundary to the upper unit, thick bands with clayey silt

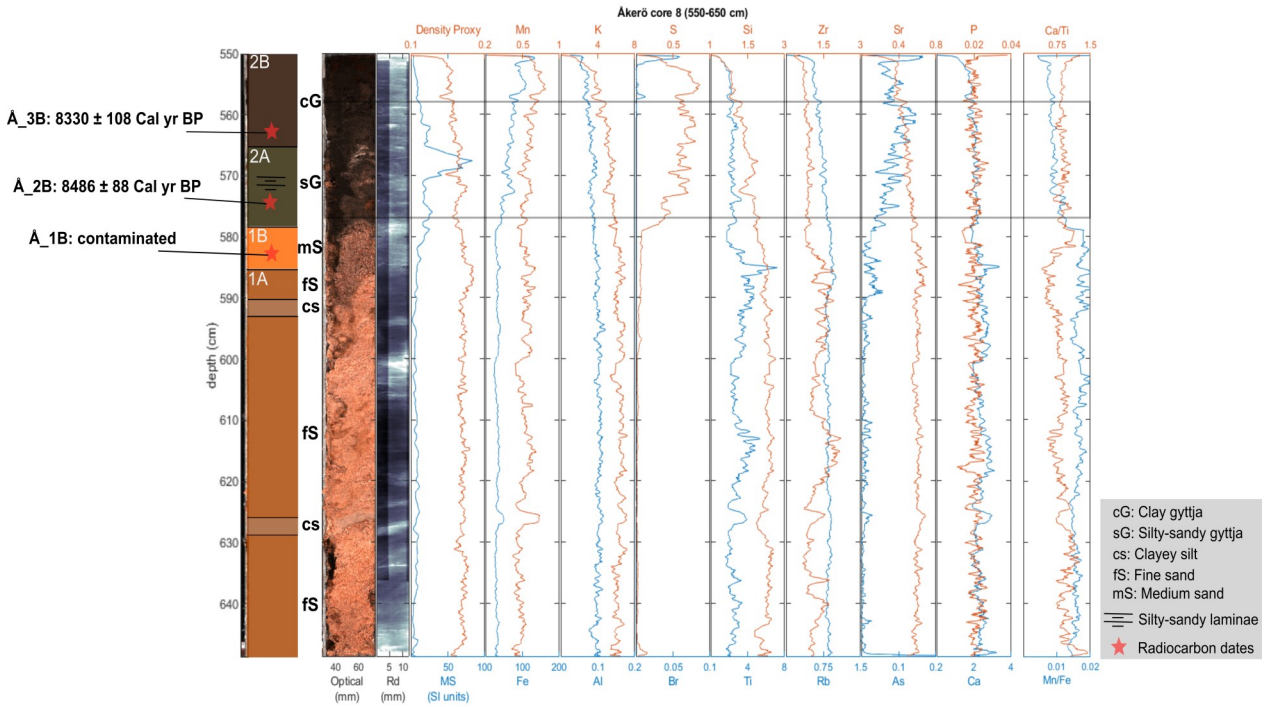

Fig. 8. Overview of core 8 (550 – 650 cm) from the Åkerö sediment record. From left to right, the log of lithology with assigned units, radiocarbon, and pollen samples. The optical and radiographic (RD) image, density, magnetic susceptibility (MS), relative concentrations of typical elements for lake surveying, Ca/Ti and Mn/Fe proxies. The box indicates a zone with an unusual signal.

bed. The presence of medium sand indicates a shift to higher energy conditions. Therefore, units 1A and 1B must be of fluvial origin. The gradual/erosional boundary to the overlying silty gyttja (2A) marks the transition from an open channel to an enclosed water body. After that, there is a gradual depletion in the coarse fraction of the sediments towards unit 2B and clay gyttja. The newly formed pond became richer in fine-grained organic matter in unit 2C, and the occasional thick bands of interbedded minerogenic material may indicate slump events from the steep walls around the pond. In unit 2D, the coarse detritus gyttja signals a shallowing of the basin. The depth of the pond at the coring site had become shallow, and primarily autochthonous organic material was deposited. Then, the transition to unit 3A suggests that telmatic vegetation took over, and peat started to accumulate in the basin (units 3B to 3D). More stable ground provided a good foundation for the settlement of trees, and the vegetation transformed into a forest (unit 3E).

3.2 Sediment chronologies

Heden: - The results of radiocarbon dating for the Heden record are presented in Table 3. A selective pollen analysis was also applied to compare the radiocarbon dates of Heden with a nearby site. The presentation and analysis of pollen are part of the chronological interpretation of the Heden record.

Heden, interpretation: Radiocarbon dating at Heden exhibits a peculiar trend in that the ages of the ^{14}C dates of deeper buried sediments in the two lowermost units appear younger than the overlying units, in a way that the first sample is younger than the second and both are younger than the third. The prospect of having contamination by reservoir or hard-water effect (MacDonald et al. 1991) in the uppermost samples seems unlikely since the sequence of the remaining four radiocarbon dates from unit 2B to 2G of the Heden record are in chronological order, and the inferred age model implies a steady sedimentation rate

Table 3. Complete list of AMS ^{14}C dating results and calibrated ages of terrestrial macroscopic plant remains from the Heden and Åkerö sediment records sorted by sample number.

Site	Depth (cm)	Sample no.	Lithology (unit)	Dated Materials	Lab code	Technique	Weight (mg C)	^{14}C date	Calibrated age (years BP)
Heden	825-819	Hed-1	sand (1)	roots, twigs	LuS_15169	AMS	1.1	7165 ± 40	7984 ± 72
	818-817	Hed-2	gyttja (2A)	roots, twigs	LuS_15170	AMS	1.2	8225 ± 40	9191 ± 152
	815-808	Hed-3	gyttja clay (2B)	twigs, bark, stems, seeds, insects	LuS_15171	AMS	1.0	8955 ± 45	10,079 ± 190
	739-735	Hed-4	clay gyttja (2D)	twigs, bark, stems, seeds, insects	LuS_15172	AMS	0.6	8445 ± 45	9477 ± 74
	647-645	Hed-5	algae-rich gyttja (2E)	twigs, bark, stems, seeds, insects	LuS_15173	AMS	1.1	7590 ± 40	8396 ± 56
	335-333	Hed-6	coarse detritus gyttja (2G)	small twigs, bark, fruits, spores, flower stem	LuS_15505	AMS	1.5	4125 ± 40	4671 ± 87
Åkerö	594-583	Å_1B	fine/medium sand (1)	twigs, bark	LuS_15672	AMS	0.5	1255 ± 40	contam.
	579-575	Å_2B	silty-sandy gyttja (2A)	bark, stems, twigs, fungi	LuS_15673	AMS	1.3	7700 ± 45	8486 ± 88
	564-561	Å_3B	clay gyttja (2B)	bark, twigs, fungi, leaf fragment, fruit	LuS_15674	AMS	1.7	7520 ± 45	8330 ± 108
	530-528	Å_4	clay gyttja (2B)	spores, twigs, bark, insect	LuS_15378	AMS	1.4	6960 ± 40	7791 ± 56
	480-478	Å_5	fine detritus gyttja (2C)	leaf fragments, twigs, bark, moss stems	LuS_15379	AMS	1.4	6200 ± 70	7098 ± 92
	430-428	Å_6	fine detritus gyttja (2C)	fruit cell, leaf fragments, twigs, bark, seed cell	LuS_15380	AMS	1.6	5640 ± 35	6416 ± 46
	380-378	Å_7	moss peat (3A)	twigs, moss, spores, leaf fragments	LuS_15381	AMS	1.5	3655 ± 45	3985 ± 68

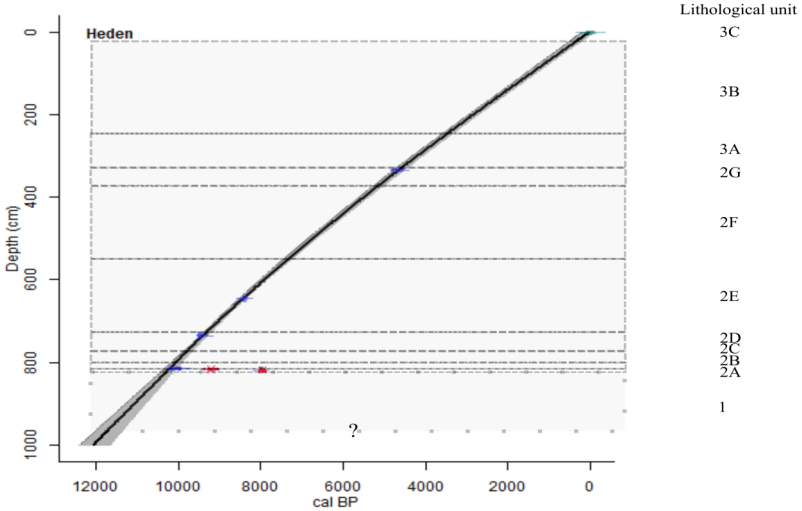

Fig. 9. Age-depth model for the sediment record from Heden. The model is extrapolated to 10 m below the surface. Radiocarbon dates not included in the model are shown in red. The lower boundary of unit 1 is marked with a question mark because the exact depth is unknown.

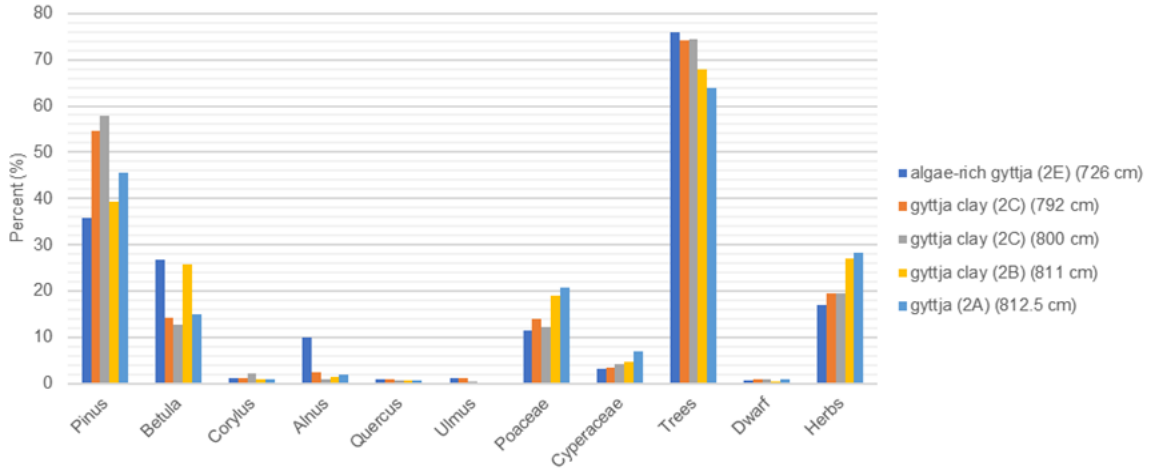

Fig. 10. Pollen frequencies of major plant taxa from selected depths, contributing additional dating control to the lower part of the Heden sediment record.

(Fig. 9). The anomalously young ages of the two samples in unit 1 and 2A indicate earlier contamination by organic material of a younger age or contamination of the samples during or after extraction. These two radiocarbon dates were therefore excluded from the age model.

The pollen analysis of the lowermost units (Fig. 10) of the Heden record demonstrates a high abundance of tree species that gradually increase up-core. *Pinus sylvestris* was most probably the dominating tree in the landscape, with *Betula nana* as an essential component. Increases in *Pinus* pollen coincide with decreases in *Betula* and vice versa. Different herbs, along with *Poaceae* and *Cyperaceae,* are also present but decrease as tree taxa increase. The pollen percentages show that *Alnus glutinosa* appears in meaningful concentrations (that is, probably established) in the last sub-sample of the analysis.

The analysis indicates that a partially forested landscape with open space for grasses and herbs gradually turned into a landscape with denser tree-cover. The pollen diagram from a detailed pollen record from Lake Holtjärnen (60°39'6.79"N 14°55'35.33"E) at 232 m a.s.l. and about 10 km to the SW from Heden suggests that *Alnus* settled and started to expand at approximately 9700 cal yr BP (Giesecke 2005). The timing of the increase in *Alnus* frequency at Lake Holtjärnen can be used as a basis for additional chronological control of the Heden sediment record. The uppermost pollen sample (H_5) at 726 cm depth, which shows a significant frequency of *Alnus,* can be interpreted as younger than 9.7 cal kyr while the samples from greater depths with negligible frequencies of *Alnus* are likely to be older than 9.7 cal kyr.

Åkerö: - The results of radiocarbon dating for the Åkerö record are presented in Table 3.

Åkerö, interpretation: The age-depth sequence for all the samples, but the bottommost is in good order (Fig. 11). It appears that the deposited sediments within the old channel at Åkerö change from fluvial sand in unit 1B to gyttja in unit 2A around 8.5 cal kyr BP. However, the lithological boundary is erosive, which suggests that the rerouting to Leksand and closure of Åkerö may have happened slightly earlier. The age-depth curve shows that during the gyttja deposition period, there was rapid sedimentation. Somewhat before the appearance of coarse detritus gyttja (unit 2D), sedimentation rates significantly decrease. Final-

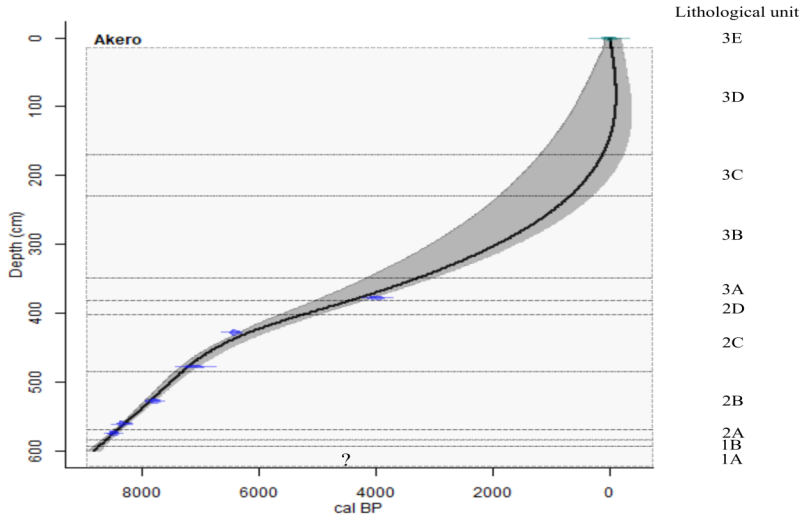

Fig. 11. Age-depth model for the sediment record from Åkerö. The model is extrapolated to 6 m below the surface. The lower boundary of unit 1A is marked with a question mark because the exact depth is unknown. Towards the top of the age-depth model, the spline has high curvature, which is unrealistic.

ly, rates of accumulation in the uppermost units of peat (units 3C to 3E) appear enormous, and they show an unrealistic backward trend towards the top. At the same time, there is a large margin of error after unit 3B.

3.3 Magnetic susceptibility and density

Heden: - The observed correlation in the magnetic susceptibility signal in the overlapping sections of the cores indicate frequent, small offsets of 6 mm that can reach up to 88 mm. The lowermost sandy unit (1) shows a gradual increase in magnetic susceptibility (MS), after which there is a drop in the highly organic gyttja (unit 2A) (Fig. 6). The next layer, gyttja clay (unit 2B), shows a dramatic increase in the magnetic susceptibility in the laminated part, followed by a dramatic decline. After that, the magnetic susceptibility gradually decreases (Fig. 7; Appendix 1-5). However, it shows a small increase in the part with silty lenses (Fig. 7; Appendix 1). The sediments show an overall gradual density decrease upwards. Furthermore, there are long intervals without any significant fluctuations. Nevertheless, there are two abrupt changes to lower and higher density in the gyttja and gyttja clay units (2A and 2B), respectively (Fig. 6).

Heden, interpretation: MS usually reflects either the intensity of erosion in the catchment area (Snowball 1996) or more local changes on the basin floor (Ojala and Saarnisto 1999). Fluctuations in the magnetic signal in Heden appear to be triggered by the in-wash of detrital material. Overall, the lithological units are uniform, do not show any interbeds, and no lenses are observed in the overlying algae-rich gyttja (unit 2E). MS signal, especially after 680 cm, gradually decreases up-core. Thus, the deposition of detrital magnetite also decreases. The most dramatic fluctuations are seen in units 2A (MS-low) and 2B (MS-high). The MS signal, along with the lithological characteristics of these units suggest post-depositional changes in the sediments due to the chemical and biological conditions in the basin (Thomson et al. 1975). In unit 2A, the low MS signal can stem from the dissolution of magnetite particles due to reduction processes from the decomposition of organic matter (Snowball 1996), while in unit 2B, the high signal can be accounted to greigite authigenesis (Snowball and Thompson 1990; Snowball 1994; Snowball 1996).

Åkerö: - The observed correlation in the magnetic susceptibility signal in the overlapping sections of the cores indicate frequent, small offsets of 20 mm that can reach up to 88 mm. MS is low and stable in the fine sand (unit 1A), slightly increases in the medium sand (unit 1B), and increases abruptly in the silty-sandy gyttja (unit 2A) (Fig. 8). After that, the signal fluctuates but gradually decreases (Appendix 6-8). In sections with higher minerogenic content like at parts with lenses or interbeds of higher minerogenic content, the magnetic signal momentarily increases. There is an overall gradual decrease in density upwards in the sequence; however, at intervals when minerogenic content and MS increase, density also appears to increase.

Åkerö, interpretation: The in-wash of minerogenic detrital material with magnetic properties controls the MS fluctuations at Åkerö. The overall decreasing trend is interrupted by frequent periods of relatively higher MS. Erosion processes and surface runoff at the steep walls of the channel occasionally deposited material that infilled the erosional bottom of the old channel at more rapid sedimentation rates like through slump events.

3.4 XRF elemental scanning

Heden: - The XRF analysis of the lowermost core in Heden shows an abrupt change in the signal of most of the elements between units 2A and 2B (Fig. 6). Fluctuations of smaller magnitude are also observed up-core. The most distinct are from 680 cm to 665 cm, and from 645 cm to 625 cm in unit 2E (Fig. 7; Appendix 1), and from 335 to 320 cm in unit 2G (Appendix 4 and 5). Otherwise, there are short-term fluctuations and long-term gradual changes in the relative concentrations of the elements. During the data fluctuations, most of the examined elements respond with either positive or negative trends. The most distinctive patterns in the data are observed in Mn, Fe, K, Si, Ti, Zr, Rb, and Sr and to a smaller extent in Al, S, Br, As, P, and Ca (Fig. 6 and 7; Appendix 1-5).

The elemental ratio proxies record significant variations in units 2A and 2B (Fig. 6), and after that, frequent but smaller in scale variations up-core. Especially at 720 cm, after the transition to algae-rich gyttja and for the rest of the record of core 9 (Fig. 7), variations in the ratios of the elements appear with high frequency and are substantial in magnitude.

The correlation coefficient analysis of the XRF data shows that most elements have a strong correlation (above 0.5) with at least one additional element (Appendix 9). Only Ar, Ni, Br, Y, and Mo do not show a strong correlation with any other element. Furthermore, principal component analysis (Fig. 12; Appendix 10 and 11) of the 13,303 data rows (depth) indicates that the first component explains 33.4 % of the variation, and the elements Al, Si, K, Ca, Ti, Mn, Fe, Zn, Rb, Sr, Zr, and Ce are strongly correlated. While elements like Cu and Ni are negatively correlated. The second component explains approximately 14 % of the variation, and the elements P, Cr, Fe, As, Tm, and Nd are strongly correlated.

Heden, interpretation: Based on some of the known properties of the investigated elements and the PCA results, a relation between element occurrence and deposition processes may be es-

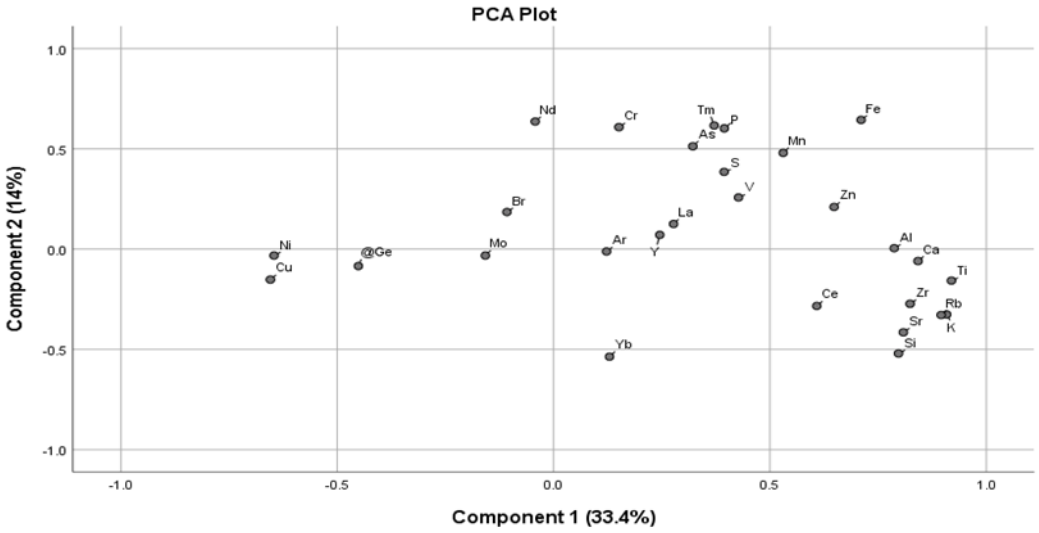

Fig. 12. Principal component analysis of XRF data from the plot of Heden sediment record with the two significant components that explain 47.4 % of the variance.

tablished. The first component may be related to the deposition of allochthonous lithogenic material that constitutes the product of erosion and weathering of rocks. Hence, elements like Cu, which are associated with organic matter, are negatively correlated. The elements of the second component seem more variable and may be connected to water geochemistry, nutrient, and oxygen levels, detrital rare earth elements, and sediment province.

Thereby, the first, dramatic change in units 2A and 2B with the reduction in the first component elements (but Fe and Mn, which increase) is likely related to a decrease in the deposition of detrital lithogenic material. Furthermore, by investigating 2A and 2B separately, there is a transient increase in Fe, S (and MS) in the beginning (Fig. 6), which probably marks the transition from unit 1 to unit 2A. At the same time, there is an increase in Br, which is the only element that is high throughout unit 2A. Bromine is linked to detrital organic matter, the formation of sediments under saline conditions, and sea-spray (De Vos and Tarvainen 2006; Davies et al. 2015). Bromine does not show a significant correlation with any other element, and it is very unlikely to indicate marine influence because Siljan had briefly been under freshwater during the Ancylus Lake Stage (von Post 1934; Möller 2006). Therefore, it is more likely that the peak in Br is related to the increase in the input of detrital organic matter along with the decrease in the relative concentration of other elements found in detrital material with high minerogenic content (Rydberg and Martinez-Cortizas 2014). The high Ca/Ti ratio indicates drier conditions or a low stand in the lake level, and the low Mn/Fe ratio is indicative of low oxygenated water probably due to poor ventilation in connection to the massive input of organic matter.

A transient increase in Fe, S, As, P (and MS), and an increase in Mn (with weak, 0.48, significance to component 2), marks the transition to unit 2B. Iron is related to MS and authigenesis (Rothwell and Croudace 2015b), which can explain the presence of greigite in 2B. At the same time, a high concentration of S indicates reducing conditions in the sediments (Rothwell and Croudace 2015b) and an anoxic environment (Harff et al. 2011). Phosphate is linked to nutrient enrichment (Davies et al. 2015). The presence of As is indicative of the transition to anaerobic conditions and also the reduction reactions of Fe and Mn (De Vos and Tarvainen 2006). The subsequent increase in Mn after the drop in the other elements indicates a change to more oxygenated waters, which can potentially be coupled to better ventilation of the water column due to lake-level lowering or enhanced biological productivity (Kylander et al. 2011). The transition to well-oxygenated waters is also marked by the increase in Mn/Fe. The increase in the second component elements is thus very likely to reflect broader environmental changes in the lake system that triggered an enhanced geochemical activity in the sediments and formed megascopic chemical laminae (Rothwell and Croudance 2015b), which are marked by the peaks in the XRF signal. Furthermore, there is a substantial increase in the Ca/Ti ratio, which may point out that environmental changes are related to a high stand in the lake level.

The fluctuation in the XRF data from 680 to 665 cm in unit 2E (Fig. 7) should be related to either the climate, a stochastic event, or generally a combination of environmental conditions that favoured erosion in the surroundings of the catchment. There is a gradual increase in most of the elements from component 1 (and MS), and there are direct observations of minerogenic lenses within the gyttja. The Ca/Ti, and Mn/Fe ratios show an abrupt drop and after, a gradual increase during the interval, which can reflect a high stand with low ventilation in the lake system followed by a lake level lowering and better ventilation. At 645 cm in unit 2E (Appendix 1) is the shallowest position in the sedimentary record where silty lenses are observed, and from 645 to 625 cm, there is a slight increase and then a gradual, relatively more distinct decrease. Finally, the XRF fluctuation from 335 to 320 cm in unit 2G (Appendix 4 and 5) is signified by an earlier interval where the XRF scanner was off due to

intense variations on the surface of the coarse detritus gyttja. Nevertheless, most of the elements show higher relative concentrations, which can probably be explained by an increase in detrital input.

Åkerö: - In the Åkerö record, there are short-term fluctuations and gradual, long term changes in the relative concentrations of the elements. At the transition from unit 1B to 2A, there is a distinct change to most of the elements, but there is neither an abrupt nor a massive response in all of them (Fig. 8). However, most of the elements (and MS) start a continuous decrease from the silty-sandy gyttja unit (2A) or just above in the clay gyttja (unit 2B). The elements that show a decreasing trend throughout the sequence are Al, Si, P, K, Ca, Ti, Rb, Sr, Zr, Zn, Ce, and Yb. At the same time, the elements Mn, Fe, Br, La, and Nd increase substantially. The relative concentrations of As and Ni decrease but then quickly rise again while Cu shows a very gradual increase. The element ratio proxies also mark a change in the transition to the lacustrine environment with Ca/Ti to show an increasing trend and Mn/Fe a decreasing trend.

Furthermore, there are short-term fluctuations in the sections with higher in-washed minerogenic material. In these layers, the primary trend reverses, and elements that decrease start to increase and vice versa.

The correlation coefficient analysis shows that most elements have a strong correlation (above 0.5) with at least one additional element (Appendix 12). The elements P, S, Ar, Mn, Y, and Mo do not show a strong correlation with any other element. Furthermore, principal component analysis (Fig. 13; Appendix 13 and 14) of the 3,951 data rows (depth) indicates that the first component explains 45.3 % of the variation, and the elements Al, Si, K, Ca, Ti, Zn, Rb, Sr, Zr, Ce, and Yb are positively correlated. At the same time, Cr, Fe, Ni, Cu, As, Br, La, Nd, and Tm are negatively

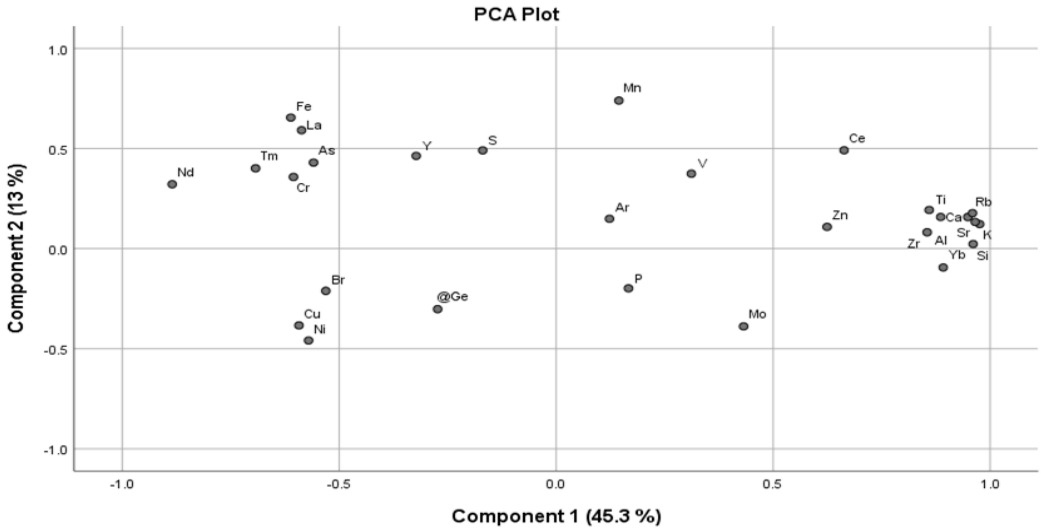

Fig. 13. Principal component analysis plot of XRF data from the Åkerö sediment record with the two significant components that explain 58.3 % of the variance.

associated. The second component explains approximately 13 % of the variation, and the elements Mn, and La are strongly correlated.

Åkerö, interpretation: There is a clear-cut separation between elements related to the deposition of allochthonous lithogenic material and elements with other established relations. Positive and negative correlations explain a substantial percentage of the data in the first component. The positively correlated elements are related to the minerogenic detrital matter that is carried to the basin by erosion-transport-deposition processes. The apparent closure of the channel after the transition from the fluvial sand unit (1A and 1B) to the gyttja unit (2A), prevented the transport of elements that would otherwise be deposited and led to a low stand (Ca/Ti increase) with poorly ventilated waters (Mn/Fe decrease). The negatively correlated elements either increase in relative concentration due to the gradual decline in the abundance of the transported detrital matter, due to surface runoff from the catchment area of the newly formed pond or due to a new geochemical regime that is triggered by the shift to an enclosed basin. The short-lived, higher concentrations in the positively correlated elements of the first component in sections with interbeds are explained by events of massive sedimentation that occur in slumps.

3.5 Carbon and Nitrogen analysis

Carbon and nitrogen analyses were only conducted on the Heden cores.

Heden: - The Heden record (Fig. 6) shows initially a very high C/N ratio together with high C content in the gyttja of unit 2A. A dramatic drop follows it in both units of gyttja clay (2B and 2C) due to a significant decrease in C content and a relatively smaller decrease in N content. In the clay gyttja unit (2D), there is a gradual increase in both C and N. In the algae-rich gyttja (2E), there are two brief intervals of declining organic matter content. However, the C/N ratio is not affected significantly (Fig. 7). After the initial fall in unit 2A, the C/N ratio remains slightly

above 10.

Heden, interpretation: The fluctuations in the ratio of total carbon to total nitrogen in the sediments are usually perceived to reflect the proportion of lacustrine and terrestrial organic material (Meyers and Ishiwatari 1993). In unit 2A, even though gyttja is typically formed in lake systems, the C/N ratio, which is at 20, indicates a significant amount of organic matter of terrestrial origin (Meyers and Ishiwatari 1993; Liiv et al. 2019). Thereby, there is an in-wash of land-derived organic material from the catchment. In units 2B and 2C, both elements appear in reduced concentrations, which indicate a relatively lower content of organic matter in the sediments. At the same time, the C/N ratio is slightly above 10, which reflects the dominance of autochthonous organic matter in a mixture of non-vascular plants, like aquatic algae, with vascular plants (Liiv et al. 2019) which are common observations to lakes (Meyers and Ishiwatari 1993). Despite the gradual increase in both C and N in unit 2D and especially in unit 2E, the C/N ratio remains slightly above 10. The intervals in unit 2E with declining carbon and nitrogen contents in the sediments can indicate periods of reduced aquatic productivity and reduced terrestrial organic matter input from the catchment.

4 Discussion

4.1 Overview and synthesis

The present study applies different methodologies to test the hypothesis that Lake Siljan was covering a greater area after its isolation from the Ancylus Lake stage and that the water level of ancient Lake Siljan was abruptly lowered (by c. 6 m - from 168.5 m a.s.l.) by a drainage event caused by the opening of a new outlet (von Post 1934). According to von Post (1934), the aftermath of the event was the abandonment of the Åkerö channel and the isolation of the basin in Heden. The results of this study provide support for the view that both Åkerö (Fig. 3) and Heden (Fig. 4) sites were once part of a more extensive lake system than today. The presence of gyttja in the collected sedimentary sequences is a manifestation of the development of a lacustrine environment (Schnurrenberger et al. 2003). However, the initial conditions of the inception of the lacustrine environment at the two sites are distinct. The distinct character of each location within the lacustrine system means that if at some point, both areas were part of the same system, it would presuppose different environmental dynamics that would produce different sedimentary sequences between the two locations. In other words, the initiation of gyttja deposition at Åkerö (Fig. 8 and Fig. 17A) marks the end of the operation of the Åkerö channel as the outlet of River Österdalälven and the shift to an isolated waterbody where low-energy conditions enabled the accumulation of fine-grained organic-rich sediments. Hence, if both Heden and Åkerö were part of the same system, it would be before the abandonment of the Åkerö channel at approximately 8.5 cal kyr BP and after the initiation of deposition of gyttja at Heden, at c. 10 cal kyr BP.

The findings from the Heden record suggest that the transition from glaciolacustrine sediments (sandy-silty sediments) to lake sediments (gyttja) occurred at around 10 cal kyr ago (Fig. 6 and Fig. 14). The initiation of this lacustrine phase must have happened sometime after the local deglaciation, which occurred c. at 10.6 cal kyr BP according to Stroeven et al. (2016) (Fig. 15A). The varve chronology constructed by Fromm (1991) suggests that the entrance to Lake Siljan just north of Leksand was at varve year 580 in the Swedish varve chronology, which corresponds to 10.5-10.6 cal kyr BP (Möller 2006), i.e., in agreement with the view of Stroeven et al. (2016). The Ancylus Lake inundated the Siljan basin in connection to the deglaciation (Fig. 15B). According to the shore level database in SGU's map finder (http://apps.sgu.se/kartgenerator/maporder_en.html, module 'shoreline map'), the Siljan basin became isolated from the Ancylus Lake at around 10 cal kyr BP (Fig. 16), i.e., more or less at the indicated age of initiation of gyttja deposition in the Heden basin.

Before the gyttja stage, the cored location does not demonstrate the occurrence of any varved sediments, which would have been expected to have been deposited in ancient Lake Siljan soon after the deglaciation. This assumption is based on the fact that varved sediment successions are recorded from Lake Orsasjön (Per Möller, personal communication, 2020) and the presence of varved sediments in Lake Siljan will be investigated during a field campaign in summer 2020 (Möller in progress). Deglaciation in Siljan area was unusual in comparison to central Sweden (Calles 1985), a multitude of glaciofluvial channels was formed (Gustavsson and Kolstrup 2009), and there is a large number of dead-ice hollows and stagnant ice fields, often buried below glaciofluvial outwash material (Nordell 1984). Accordingly, the most plausible explanation for non-existing varved sediments below the gyttja in the Heden basin is that an ice block was buried in the basal subaqueous sediments of the area.

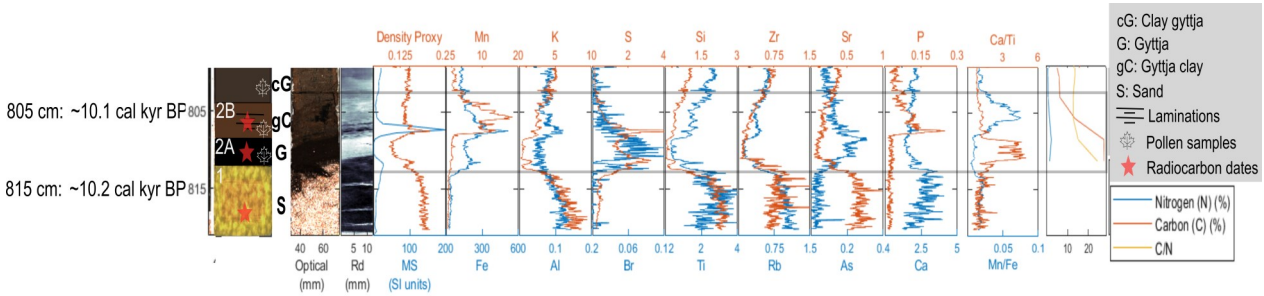

Fig. 14. Selected part of core 11 from the Heden record with the assigned ages according to the age-depth model.

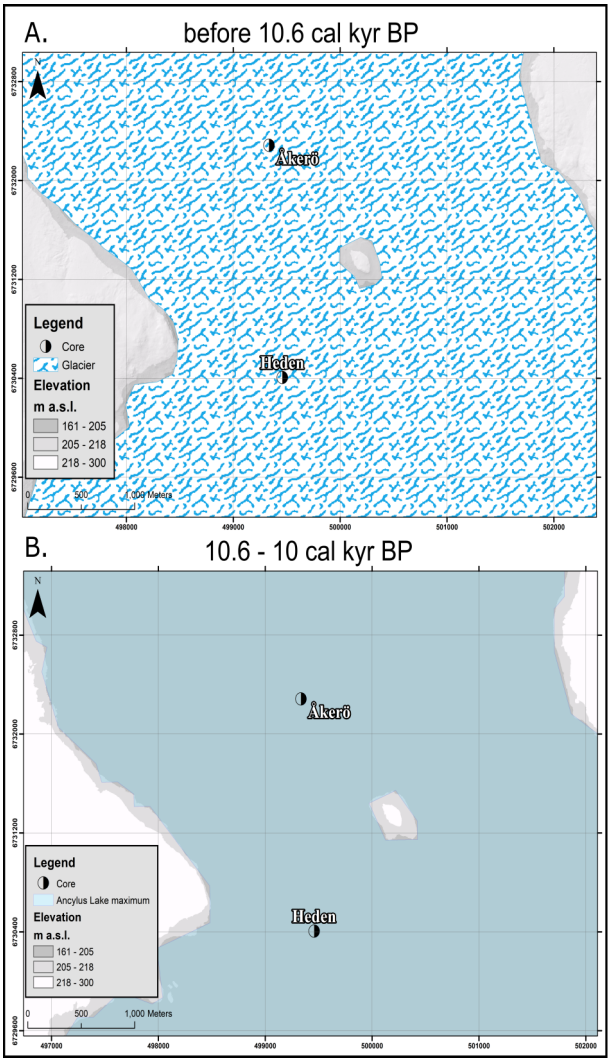

Fig. 15. Lake Siljan evolution stages of the SE outlet area at present Leksand until 10 cal kyr BP. A. The area before 10.6 cal kyr BP and slightly after the start of deglaciation. Higher elevated areas are the first to be uncovered. B. The Ancylus Lake ingression takes place around 10.6 cal kyr BP and lasts approximately until 10 cal kyr BP.

After its melting and the creation of the Heden basin the formation of varved sediments had ceased and gyttja was deposited directly on the glaciolacustrine subaqueous fan deposits. The hummocky topography of these deposits in the surrounding area suggests numerous occurrences of buried ice blocks, which also is indicated on the SGU map of the area.

Accordingly, the sandy unit (1) in the Heden record, as is also characterized by the Geological Survey of Sweden (Fig. 1A), is related to meltwater during deglaciation, and more specifically underflows that gradually deposited material to build up subaqueous fans (pers. comm. P. Möller). Above a possible depositional hiatus (due to burried iceberg melt) is Unit 2A, which is a gyttja with a high percentage of organic material (C-N analysis, Fig. 6 and Fig. 14). This can be interpreted as the product of redeposition processes during water level changes. Changes in the hydrological conditions and ventilation of the lake are also indicated by the elemental ratios (Ca/Ti and Mn/Fe). As a result of the chronology in unit 2B and the structure of the sediments of the units 1 and 2A at the bottom of the Heden record can form the evidence of the transition to ice-free conditions and possibly the Ancylus Lake ingression. Nevertheless, the dates of these units are erroneous due to either contamination or natural causes, and the extrapolation of the age-depth model based on the reliable radiocarbon-dated ages of the upper samples may not show high accuracy. Hence, this scenario needs further investigation.

Even though the results from Heden appear to be particularly interesting in units 2A and 2B due to the abrupt transitions in most of the analysed data, the most relevant units regarding the question in scope are units 2D and 2E (Fig. 7 and Fig. 17B). The factor that seems to place the drainage event to these units is the timing of the abandonment of the former outlet at Åkerö, at 8486 cal kyr BP or according to the age-depth model of Åkerö, precisely at the transition to 2A (579 cm), at 8547 cal yr BP (Fig. 11). The increased frequency of *Alnus* in the pollen record from Heden at 726 cm (Fig. 10) is close to the radiocarbon age of 9477 cal yr BP at approximately 735 cm (Table 3; Fig. 6). Moreover, the timing of the appearance of *Alnus* in the pollen record of the proximate Lake Holtjärnen (c. 7 km SW of Leksand) is at 9.7 cal kyr BP (Giesecke 2005). Hence, the radiocarbon date of 9477 cal yr BP at 735 cm constitutes the trustworthy age that is placed earlier than the transition in the sediments of Åkerö at 8.5 cal kyr BP.

At Heden, after the massive input of organic matter with high C/N ratio content in unit 2A, and the dramatic decrease in the relative concentration of most

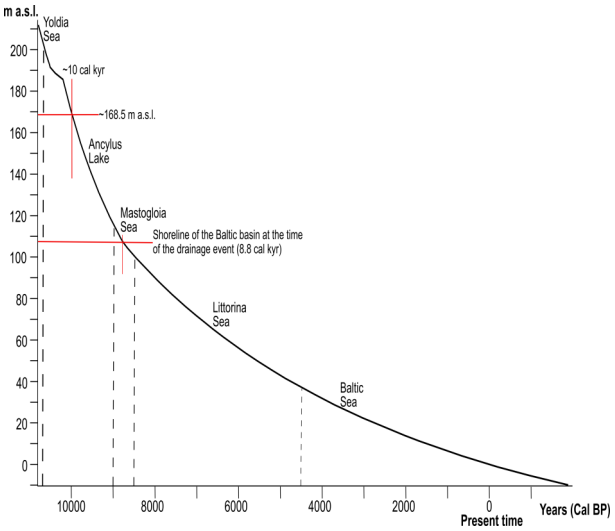

Fig. 16. Shore-level displacement diagram for the Siljan region based on the isostatic uplift and sea-level fall for the past 10 kyr and with projection to the future. Shortly after 10 cal kyr BP, the Ancylus Lake regression passed the 168.5 m threshold indication of the isolation of the Siljan basin and the formation of ancient Lake Siljan. The time of the drainage event corresponds to a late stage of the Mastogloia sea, where the shoreline of the Baltic basin was slightly lower than 110 m a.s.l. The figure is a re-drawn and modified version of the original produced by the Geological Survey of Sweden (SGU) and the shore level database in SGU's map finder. The timings of the different Baltic Sea stages are adapted from Björck (2008).

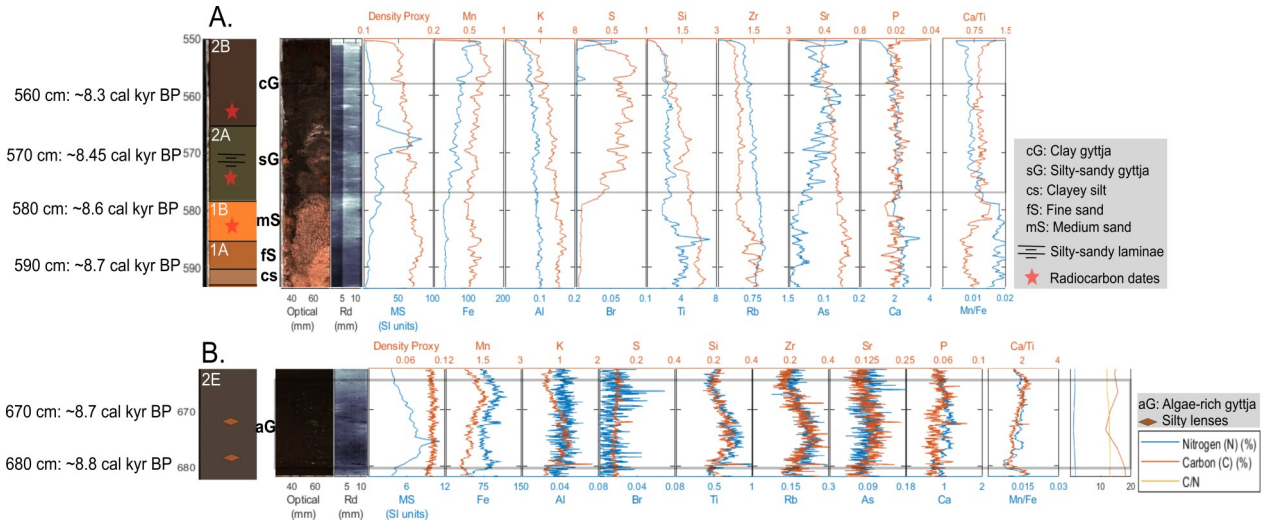

Fig. 17. Selected parts from the Heden and Åkerö records with assigned ages according to the age-depth model. A. The transition to the gyttja sequence in core 8 of Åkerö (Fig. 8). B. The interval in core 9 of the Heden record that corresponds to the drainage event.

elements but Br and As (Fig. 6), there is a trend to higher elemental concentrations and stabilization. Later, changes in the concentration appear to be more restrained apart from the transition to algae-rich gyttja (2E) (Fig. 7), where there is a gradual reduction and stabilization of most of the PCA component 1 elements of detrital origin (Fig. 12). Subsequently, there is a peculiar trend in the concentration of detrital elements at 680 cm, lasting up to 665 cm. Additionally, this fluctuation in the XRF data is accompanied by a peak in magnetic susceptibility and a significant decrease in the organic matter content (Fig. 7 and Fig. 17B). Interestingly, the reduction in C concentrations occurs after an earlier period of increasing concentrations, which can be accounted to the input of organic matter from the vegetated soils (Paus et al. 2019). The increase in MS occurs after a previous period of decreasing MS signal. Moreover, there is also a slightly higher sediment density, and the sediments contain more frequent silty lenses. The response of Ca/Ti and Mn/Fe proxies is also peculiar and show an abrupt decrease at 680 cm, followed by a more gradual increase. The most significant changes in the element ratios come in two steps. The first starts simultaneously with the increase in the C content at approximately 690 cm, and the second comes after an interval of stability and slightly earlier than the increase in the minerogenic matter and the decrease in C content at 680 cm. The response of the record within the interval of 680 to 665 cm may indicate the initiation of a period of increased input of eroded material from the catchment of Siljan and stronger water circulation in the lake. The trend toward higher concentrations is observed after a short and abrupt peak in most of the elements of minerogenic detrital origin at approximately 679 cm.

The age-depth model of Heden (Fig. 9), places the start of the period with increased organic matter input (690 cm) at 8.9 cal kyr BP, the time of decrease of the elemental ratios (680 cm) and the beginning of the period with increased minerogenic sedimentation (679 cm) at c. 8.8 cal kyr BP. At 8.65 cal kyr BP, the XRF elemental data, MS, and C-N proxies have already come back to typical values and start a very gradual decreasing trend up-core (Appendix 1-5). Nevertheless, the distribution of the occurrence of catastrophic drainage over 100 years seems contradictory as this most probaly was a very short event of erosion at which overflowing water from the Siljan basin cut a new outlet north of the Åkerö channel. Hence, more attention should be paid on the exact point in the record where elements of detrital origin have a more profound signal at 679 cm. Therefore, the gradual and smooth curve that is observed after 679 until approximately 668 cm represents a long chronological period in the Heden sediment record that must reflect the effect of the drainage; the lake level drop lead to exposure of barren lake sediments and thus mobilization of clastic sediment into the Heden basin, interbedding with the deposition of gyttja. This exposure of formerly submerged land is set to 8.8 cal kyr BP as a best guess from the age-depth model for the assigned depth from min 95% at 8745 to max 95% at 8847 cal yr BP.

4.2 Climate and hydrology

The cause of the rise in the water level of the ancient Lake Siljan leading to the drainage event and the formation of a new outlet north of the Åkerö channel is most probably a stochastic event in connection to the local climate. The current study does not use any climatic proxies, and hence, a description of the local palaeoclimate at that time based solely on XRF and C-N data is not feasible. However, it is vital to understand the climatic trends during the indicated time of the event. It is generally accepted that temperatures over Scandinavia were rising between 10 and 8.2 cal kyr BP (Borzenkova et al. 2015). At 9 cal kyr BP, oxygen-isotope data from the Abisko area in Northern Sweden, suggest warm and moist climatic conditions (Hammarlund et al. 2002). In north-central Sweden, climate reconstructions based on the pollen record of Lake Gilltjärnen indicate rapid warming from 10 to 9 cal kyr BP and is suggested that warming continued until 8.6 cal kyr BP (Antonsson et al. 2006). However, a small shift to minor cooling can also be seen earlier than 8.6 cal kyr BP in the smoothed annual mean temperature reconstructions of Antonsson and colleagues (2006). In an examination of approximately 50 globally distributed palaeoclimatic records for investigating

climate variability in the Holocene period, Mayewski et al. (2004) describe the period from 9 to 8 cal kyr BP as a time of rapid climate changes due to the "glacial aftermath." A general cooling towards the poles is suggested, which among others, is reflected by ice rafting and intense atmospheric circulation in North Atlantic and Siberia and glacier advances in Scandinavia (Mayewski et al. 2004). A study of the Holocene climate of Scandinavia based on radiocarbon dates and lacustrine data that reflect glacier variations, propose the start of a warm period around 8.6 cal kyr BP that peaks at 8.3 cal kyr BP (Karlén and Kuylenstierna 1996). Even though the relative disagreements, the changes in the climate led to the well-recognized cooling during the "8.2 kyr" event that may portray the impact of meltwater pulse in the Atlantic Ocean from Lake Agassiz (Mayewski et al. 2004; Antonsson et al. 2006; Paus et al. 2019).

It can be speculated that erosion processes were generated around 8.8 cal kyr BP. Climatic fluctuations could cause erosion in two distinct ways, first, by affecting the slope hydrology (Huggett 2011). For example, increased precipitation and stronger winds, in combination with sparsely vegetated soils, can stimulate erosion and surface runoff. Another potential factor that can cause erosion is the input of a higher volume of water in the lake, causing the lake levels to rise above the sill and then abruptly drop and expose previously submerged areas. In the first case scenario, it is not likely that vegetation was sparse at the time of the ancient Lake Siljan drainage event. Furthermore, it is difficult to accept such a smooth and long-term effect in the record of Heden purely from surface runoff in the catchment. On the contrary, the response of the elemental proxies Ca/Ti and Mn/Fe earlier than the event suggest frequent and abrupt variations in the hydrological conditions of the lake that can potentially be indicative of stochastic or seasonal water-level fluctuations. Therefore, in the case of the ancient Lake Siljan, the scenario of erosion after a higher water stand seems more plausible.

The original hypothesis by von Post (1934) postulates that the opening of the new channel came after erosion and down-cutting of the silty-sandy sediments during an exceptional high-stand in the lake-level of ancient Lake Siljan. Lake waters can rise either through more intense precipitation and snowmelt or clogging of the outflow channel. A more massive inflow of water typically results in raised lake level that is balanced by higher outflows (Bengtsson and Malm 1997). Consequently, if the inflow of water is significantly higher so that the volume of water cannot be accommodated within the contemporary outflow channel, the lake will absorb and compensate the misbalance by rising to a higher level. Historical observations of Lake Siljan show that water level can increase to 6.5 m above the sill, and recent records of seasonal fluctuations show a typical range between 1.1 to 1.7 m above the sill, which mainly occur due to upstream accumulation of snow (Bengtsson and Malm 1997).

4.3 The drainage scenario

Overall, the results of this study suggest that the ancient Lake Siljan existed for approximately 1200 years (Fig. 14 and Fig. 18A). Shore platforms and beach bluffs to the west of Åkerö can be followed into the Åkerö channel, suggesting a water level of ancient Lake Siljan at 168.5 m a.s.l. (von Post 1934) which can also be confirmed from the present-day DEM over the area (Figs. 3, 4 and 5). The sediment surfaces at the walls north and south of the Åkerö channel are at c. 175 m a.s.l. Hence, it can be speculated (von Post 1934), that the area of the present outlet for River Österdalälven was at a lower-elevation depression between 168.5 and 175 m a.s.l. At approximately 8.8 cal kyr BP, during a stochastic water level rise of the ancient Lake Siljan, the depression was flooded. The water level rise must have been in the order of 6 m or less and initiated erosion processes that led to the formation of a new, lower-situated outlet for the Siljan basin. A lake level lowering signaled the end of ancient lake Siljan and the abandonment of the Åkerö channel. Erosion processes continued to act on the landscape after the lake lowering occurred.

The increase in the minerogenic detrital matter and the decrease in organic matter content (Fig. 7 and Fig. 17B) in Heden, indicate that this lake level lowering took place at c. 8.8 cal kyr BP (Fig. 18B). The absence of shorelines from 164 to 168 m a.s.l. demonstrate the abruptness of the lowering. Simultaneously, the water flow and minerogenic matter in the water column increased, which led to the deposition of material (silty lenses in the Heden basin) originating from formerly submerged land. In Åkerö, the first sign of increased water flow is seen in the coarsening of the fluvial sand (Fig. 8 and Fig. 17A) at c. 8.65 cal kyr BP (Fig. 11), while the abandonment of the old channel is seen at the transition to lacustrine deposits at c. 8.5 cal kyr BP. However, the great dynamism in the environment of an outlet channel that responded to the drainage suggests a more volatile sedimentary record. The reduction in the minerogenic content after 8.65 cal kyr BP at Heden indicate that, by assigning the drainage at this age that the 8.5 cal kyr age for the sand at the base of the core from Åkerö is lagging somewhat behind. Therefore, the evidence of the sedimentary record of a calm environment like the basin in Heden indicates that the drainage event must have happened when the detrital minerogenic fraction increased around 8.8 cal kyr BP. If the timing of the Littorina maximum is placed between 7.6 and 6.5 cal kyr BP (Yu et al. 2007), the timing of the channel relocation to the north of Åkerö is seemingly about 1000 to 2000 years older than the original scenario by von Post (1934). However, an offset of this magnitude is a typical underestimation of sediment chronologies at that time (Fredén 1967). Furthermore, unless the proxies of elemental ratios are not fully applicable to the environmental conditions of the present study, fluctuations in Ca/Ti and Mn/Fe at the time before and after the event indicate that lake levels rose remarkably and fell in several occasions. However, the profound catastrophe that makes this stochastic event unique is the opening of the new outlet channel.

Limitations to this study are that the isolation of the Heden basin could have potentially been marked more profoundly in the analysed data and that a better chronological relation to the abandonment of the

Åkerö channel could have been established. The lake level rise can be suggested to be seen in the elemental ratios at 680 cm, however, these ratios were initially applied in other geological settings. The ratios should be combined with more sedimentary and biological observations in the lake, and they must be tested over more extended periods to increase the confidence regarding their validity. The effect of the lake level lowering is seen in the Heden record. Still, on the radiocarbon dated age of the transition to lake sediments at the Åkerö record, the Heden record only demonstrates the absence of silty lenses. Nevertheless, the drainage at 679 cm and the interval of the apparent aftermath from 679 to 665 cm in Heden, is chronologically close to the transition in Åkerö, is not repetitive, and the record, in general, constitutes this interval the right candidate for the examined scenario. The overall observations corroborate von Post's (1934) hypothesis of a higher lake-level before the drainage and the proposed magnitude of this lake level rise is supported by DEM data.

Further investigation could shed light on some

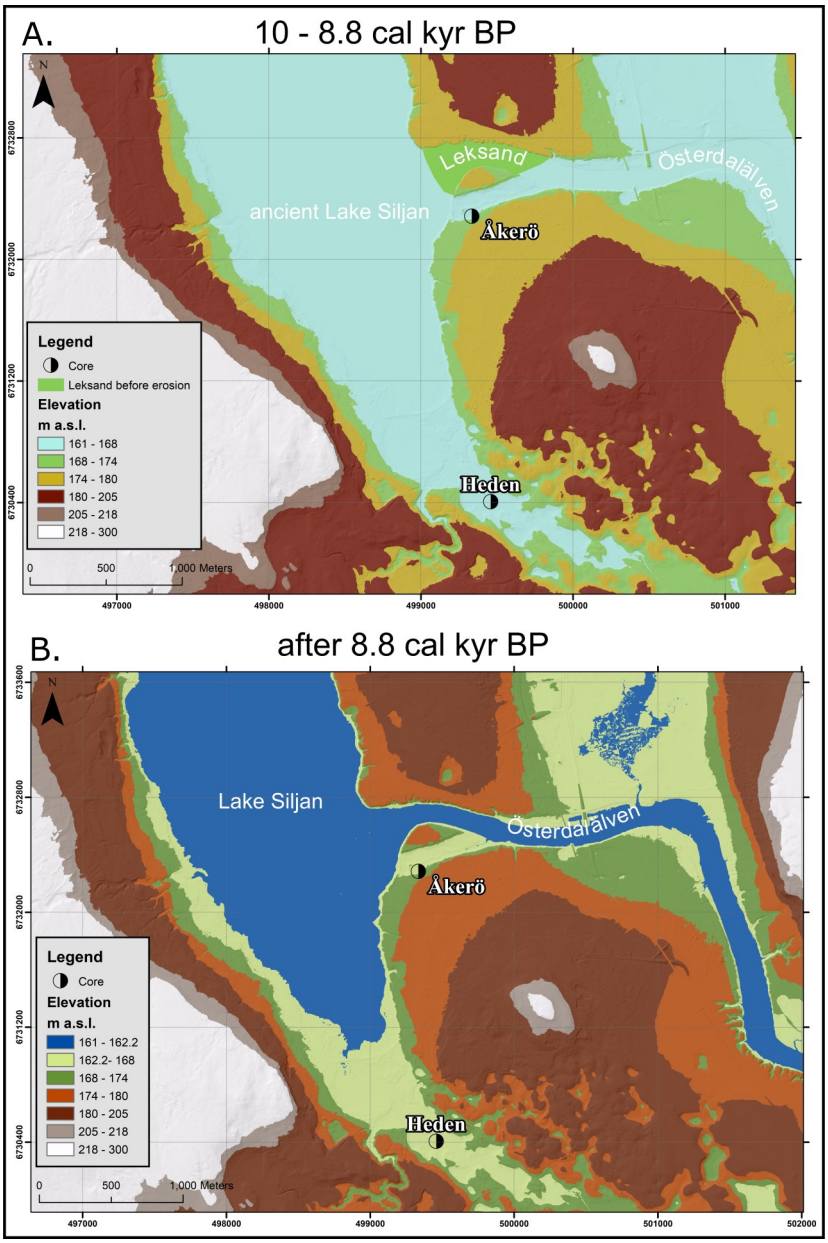

Fig. 18. Lake Siljan evolution stages of the SE outlet area at present Leksand after 10 cal kyr BP. A. Isostatic uplift on land resulted in the isolation of the Siljan basin from Ancylus Lake around 10 cal kyr BP and 168.5 m a.s.l. After the isolation, ancient Lake Siljan covered a greater area than today and drained through the now-abandoned Åkerö channel to a lake at lower altitude further to the east. This an-cient Lake Siljan phase lasted approximately until 8.8 cal kyr BP when the new outlet channel opened. B. Lake Siljan after the catastrophic drainage event. The Åkerö channel was abandoned and the Heden basin, which was earlier a part of ancient Lake Siljan, became isolated.

of the aspects of the drainage event. It would be interesting to find out more regarding the underlying causes of the higher water levels, the effect on the rates of deposition, how fast the lowering occurred, and whether it happened in more than one stage. In this respect, future studies could focus on other strategic locations for coring, identification of relict beach ridges, a more analytical reconstruction of the palaeoenvironment after 9 cal kyr BP based on pollen, diatoms, and other environmental proxies, a more extended analysis of C and N content up-core, and identification of other local proxies that could indicate lake-level changes.

5 Conclusions

The present study uses traditional and modern geological methods for the assessment of the Lake Siljan drainage scenario of von Post (1934) that encompasses the abandonment of the Åkerö channel at Leksand and the isolation of the Heden basin c. 2 km to the south. The current findings strengthen the view that an abrupt event led to the rerouting of the outlet of Lake Siljan and the separation of the Heden basin from the Siljan lake basin. The results constrain previous findings concerning the timing of the event, provide evidence of water level lowering, and suggest a connection between the lithology in the record of Heden and the isolation of the basin from Lake Siljan. In summary,

- The catastrophic drainage is placed at 8.8 cal kyr BP. The peak in the minerogenic detrital matter at 679 cm of the Heden record marks the fall in water levels. Therefore, the opening of the new channel at Leksand took place approximately 1-2 cal kyr earlier than the original scenario proposed by von Post (1934).
- The connection of the Heden basin to the Siljan basin is reflected by the silty lenses in the algae rich gyttja in the lower part of the Heden sediment core.
- The coarsening of sand at Åkerö around 8.65 cal kyr BP reflects the erosion and stronger water-flow of the drainage event, however, the sedimentary record of a channel that responded to the event is more volatile and should not be trusted chronologically.
- Future research could strengthen the present study and should focus on a more thorough investigation of proxies from additional sedimentary records, and a more analytical study of the preserved geomorphology.

6 Acknowledgements

I would like to thank my supervisor Prof. Emer. Per Möller, and co-supervisors, Prof. Dan Hammarlund, and Lect. Karl Ljung, for their invaluable advice, directions, input, and support during all the stages of this master project up to the last moment. The project was exciting and enjoyable, despite any hard times. I would also like to thank Srlect. Andreas Nilsson for the laboratory instructions in magnetic susceptibility, and all the laboratory and administrative staff at the Department of Geology of the University of Lund that contributed with their expertise to this project. Furthermore, I would like to thank adjunct academic staff Marie-Louise Siggaard-Andersen from the Globe Institute at the University of Copenhagen for sharing her knowledge and expertise in sediment analyses with XRF scanning. Many thanks should also go to all the teachers and my fellow students during the master's program. It was a pleasure to participate in all the field trips with them, and I hope to have the chance to meet again soon. Finally, I would like to thank my family and friends for all the love, support, and understanding during the last two years.

7 References

Antonsson, K., Brooks, S.J., Seppä, H., Telford, R.J. & Birks, H.J.B., 2006: Quantitative palaeotemperature records inferred from fossil pollen and chironomid assemblages from Lake Gilltjärnen, northern central Sweden. *Journal of Quaternary Science 21*, 831-841.

Bengtsson, L. and Malm, J., 1997: Using rainfall-runoff modeling to interpret lake level data. *Journal of Paleolimnology 18*, 235–248.

Björck, S., 2008: The late Quaternary development of the Baltic Sea basin. *In* H. von Storch (ed.): *Assessment of climate change for the Baltic Sea Basin*, 398-407. Springer.

Blaauw, M., 2010: Methods and code for 'classical' age -modelling of radiocarbon sequences. *Quaternary Geochronology 5*, 512-518.

Borzenkova, I., Zorita, E., Borisova, O., Kalniņa, L., Kisielienė, D., Koff, T., Kuznetsov, D., Lemdahl, G., Sapelko, T., Stančikaitė, M. and Subetto, D., 2015: Climate Change During the Holocene (Past 12,000 Years). *In* The BACC II Author Team (eds.): Second Assessment of Climate Change for the Baltic Sea Basin, 25-49. Regional Climate Studies. Springer, Cham.

Brodie, C.R., Leng, M.J., Casford, J.S.L., Kendrick, C.P., Lloyd, J.M., Yongqiang, Z. & Bird, M.I., 2011: Evidence for bias in C and N concentrations and δ 13C composition of terrestrial and aquatic organic materials due to pre-analysis acid preparation methods. *Chemical Geology 282(3)*, 67–83.

Calles, B., 1985: Water discharges during the deglaciation of the Lake Siljan basin, Central Sweden. *Geografiska Annaler 67A(1-2)*, 101-112.

Cox Analytical Systems, 2019. *Itrax XRF Corescanner brochure*. 4pp.

Davies S., Lamb H. and Roberts S., 2015: Micro-XRF Core Scanning in Palaeolimnology: Recent Developments. *In* I.W., Croudace and R.G., Rothwell (eds.): *Micro-XRF Studies of Sediment Cores: Applications of a non-destructive tool for the environmental sciences*,

189-226. Developments in Paleoenvironmental Research 17, Springer, Dordrecht, NL.

De Vos, W. and Tarvainen, T. (Chief-editors), 2006: *Geochemical atlas of Europe*. Part 2, Interpretation of Geochemical Maps, Additional Tables, Figures, Maps, and Related Publications. Geologian tutkimuskeskus (Finland) & Forum of the European Geological Surveys Directors. Geological Survey of Finland. 690pp.

Faegri, K., Iversen, J., Kaland, P. E. & Krzywinski, K., 1989: *Textbook of pollen analysis*. 4. ed. Wiley. 328pp.

Flantua, S. G. A., Blaauw, M. & Hooghiemstra, H., 2016: Supplement of Geochronological database and classification system for age uncertainties in Neotropical pollen records. *In* S. G. A. Flantua, M. Blaauw, & H. Hooghiemstra: *Geochronological database and classification system for age uncertainties in Neotropical pollen records,* 387-414. Climate of the Past 12, 15pp.

Fredén, C. 1967: A Historical Review of the Ancylus Lake and the Svea River. *Geologiska Föreningen i Stockholm Förhandlingar 89(3)*, 239-267.

Fromm, E. 1991: *Varve chronology and deglaciation in south-eastern Dalarna, Central Sweden*. Sveriges geologiska undersökning 77, 49pp.

Giesecke, T., 2005: Holocene dynamics of southern boreal forest in Sweden. *The Holocene 15 (6)*, 858-872.

Gustavsson, M. and Kolstrup, E., 2009: New geomorphological mapping system used at different scales in a Swedish glaciated area. *Geomorphology 110 (1-2)*, 37-44.

Halden, B. 1936: Isavsmaltning och strandforskjutningar i Siljansdalen. *Geologiska Föreningen i Stockholm Förhandlingar 58*, 19-89.

Hammarlund, D., Barnekow, L., Birks, H.J.B., Buchardt, B. & Edwards, T.W.D., 2002: Holocene changes in atmospheric circulation recorded in the oxygen-isotope stratigraphy of lacustrine carbonates from northern Sweden. *The Holocene 12(3)*, 339–351.

Haberzettl T., Corbella H., Fey M., Janssen S., Lucke A., Mayr C., Ohlendorf C., Schabitz F., Schleser G., Wille M., Wulf S. & Zolitschka B., 2007: Lateglacial and Holocene wet–dry cycles in southern patagonia: chronology, sedimentology and geochemistry of a lacustrine record from Laguna Potrok Aike, Argentina. *Holocene 17*, 297–310.

Harff J., Endler, R., Emelyanov, E., Kotov, S., Leipe, T., Moros, M., Olea, R., Tomczak, M. & Witkowski, A., 2011: Late Quaternary Climate Variations Reflected in Baltic Sea Sediments. *In* J. Harff, S. Björck, P. Hoth (eds): *The Baltic Sea Basin*, 99-132. Central and Eastern European Development Studies (CEEDES). Springer, Berlin, Heidelberg.

Holm-Alwmark, S., Rae, A.S.P., Ferrière, L., Alwmark, C. & Collins, G.S., 2017: Combining shock barometry with numerical modelling: Insights into complex crater formation – The example of the Siljan impact structure (Sweden). *Meteoritics and Planetary Science 52*, 2521-2549.

Huggett, R.J., 2011: *Fundamentals of Geomorphology*. 3rd edition, Abingdon, Oxon, Routledge, 516pp.

Håkanson, L. and Jansson, M., 1983: *Principles of lake sedimentology*. Springer-Verlag. 316pp.

Jouve G., Francus P., Lamoureux S., Provencher-Nolet L., Hahn A., Haberzettl T., Fortin D., Nuttin L. & The PASADO Science Team, 2013: Microsedimentological characterization using image analysis and μ-XRF as indicators of sedimentary processes and climate changes during Lateglacial at Laguna Potrok Aike, Santa Cruz, Argentina. *Quaternary Science Reviews 71*, 191–204.

Karlén, W. and Kuylenstierna, J., 1996: On solar forcing of Holocene climate: evidence from Scandinavia. *The Holocene 6(3),* 359–365.

Kylander M., Ampel L., Wohlfarth B. & Veres D., 2011: High-resolution X-ray fluorescence core scanning analysis of Les Echets (France) sedimentary sequence: new insights from chemical proxies. *Journal of Quaternary Science 26*, 109–117.

Liiv, M., Alliksaar, T., Amon, L., Freiberg, R., Heinsalu, A., Reitalu, T., Saarse, L., Seppä, H., Stivrins, N., Tõnno, I., Vassiljev, J. & Veski, S., 2019: Late glacial and early Holocene climate and environmental changes in the eastern Baltic area inferred from sediment C/N ratio. *Journal of Paleolimnology 61(1)*, 1-16.

Lowe, J. J. and Walker, M. J. C., 2014: *Reconstructing Quaternary Environments*. 3. ed. Routledge. 538pp.

Löwemark, L., Bloemsma, M., Croudace, I.W., Daly, J.S., Edwards, R.J., Francus, P., Galloway, J.M., Gregory, B.R., Huang, J.S., Jones, A.F., Kylander, M.E., Luo, Y., Maclachlan, S., Ohlendorf, C., Patterson, R., Pearce, C., Profe, J., Reinhardt, E.G., Stranne, C., Tjallingii, R. &Turner, J., 2019: Practical guidelines and recent advances in the Itrax XRF core-scanning procedure. *Quaternary International 514*, 16–29.

MacDonald, G.M., Beukens, R.P. & Kieser. W.E., 1991: Radiocarbon Dating of Limnic Sediments: A Comparative Analysis and Discussion. *Ecology 72(3)*, 1150-1555.

Mayewski, P.A., Rohling, E.E., Stager, J.C., Karlén, W., Maasch, K.A., Meeker, L.D., Meyerson, E.A., Gasse, F., van Kreveld, S., Holmgren, K., Lee-Thorp, J., Rosqvist, G., Rack, F., Staubwasser, M., Schneider, R.R. & Steig, E.J., 2004: Holocene climate variability. *Quaternary Research 62(3)*, 243-255.

Melles M., Brigham-Grette J., Minyuk P.S., Nowaczyk N.R., Wennrich V., Andreev A.A., Coletti A., Cook T.L., Haltia-Hovi E., Kukkonen M., Lohzkin A.V., Rosén P., Tarasov P., Vogel H. & Wagner B., 2012. 2.8 million years of Arctic climate change from Lake El'gygytgyn, NE Russia. *Science 337*, 315–320.

Meyers, P.A. and Ishiwatari, R., 1993: Lacustrine organic geochemistry—an overview of indicators of organic matter sources and diagenesis in lake sediments. *Organic Geochemistry 20(7)*, 867-900.

Möller, P. 2006: Rogen moraine: an example of glacial reshaping of pre-existing landforms. *Quaternary Science Reviews 25(3-4)*, 362-389.

Nordell, P. O., 1984: *Deglaciation studies in Ovansiljan, Dalarna, Sweden*. Ph.D. Thesis, Abstracts of Uppsala Dissertations from the Faculty of Science 754. Uppsala University, Uppsala, Sweden. 14pp.

Ojala, A.E. and Saarnisto, M., 1999: Comparative varve counting and magnetic properties of the 8400-yr sequence of an annually laminated sediment in Lake Valkiajärvi, Central Finland. *Journal of Paleolimnology 22*, 335–348.

Olsen, J., Anderson, N.J. & Leng, M.J., 2013: Limnological controls on stable isotope records of late-Holocene palaeoenvironment change in SW Greenland: A paired lake study. *Quaternary Science Reviews 66*, 85-95.

Paus, A., Haflidason, H., Routh, J., Naafs, B.D.A. & Thoen, M.W., 2019: Environmental responses to the 9.7 and 8.2 cold events at two ecotonal sites in the Dovre mountains, mid-Norway. *Quaternary Science Reviews 205*, 45-61.

von Post, L., 1934: Bonäslinjen. En lednivå bland Siljansbäckenets senkvartära strandlinjer. *GFF 55*, 19-59.

Ramsey, C.B., 2017: Methods for summarizing radiocarbon data sets. *Radiocarbon 59*(2), 1809-1833.

Reimer, P.J., Bard, E., Bayliss, A., Beck, J.W., Blackwell, P.G., Bronk Ramsey, C., Buck, C.E., Edwards, R.L., Friedrich, M., Grootes, P.M., Guilderson, T.P., Haflidason, H., Hajdas, I., Hatté, C., Heaton, T.J., Hoffmann, D.L., Hogg, A.G., Hughen, K.A., Kaiser, K.F., Kromer, B., Manning, S.W., Niu, M., Reimer, R.W., Richards, D.A., Scott, E.M., Southon, J.R., Turney, C.S.M. & van der Plicht, J., 2013. IntCal13 and Marine13 radiocarbon age calibration curves, 0-50,000 years cal BP. *Radiocarbon 55*, 1869-1887.

Rothwell, R. G. and Croudace, I.W., 2015a: Micro-XRF studies of sediment cores: A perspective on capability and application in the environmental sciences. *In* I.W., Croudace and R.G., Rothwell (eds.): *Micro-XRF Studies of Sediment Cores: Applications of a non-destructive tool for the environmental sciences*, 1-21. Developments in Paleoenvironmental Research 17, Springer, Dordrecht, NL.

Rothwell, R. G. and Croudace, I.W., 2015b: Twenty Years of XRF Core Scanning Marine Sediments: What Do Geochemical Proxies Tell Us?. *In* I.W., Croudace and R.G., Rothwell (eds.): *Micro-XRF Studies of Sediment Cores: Applications of a non-destructive tool for the environmental sciences*, 25-102. Developments in Paleoenvironmental Research 17, Springer, Dordrecht, NL.

Rydberg, J. and Martinez-Cortizas, A., 2014: Geochemical assessment of an annually laminated lake sediment record from northern Sweden: a multi-core, multi-element approach. *Journal of Paleolimnology 51*, 499–514.

Schnurrenberger, D., Russell, J. & Kelts, K., 2003: Classification of lacustrine sediments based on sedimentary components. *Journal of Paleolimnology 29*, 141–154.

Smith, C.A. and Peterson, G., 2014: Quaternary geomorphology of the Siljan area, central Sweden. *Journal of Maps 10(4)*, 521-528.

Snowball, I.F. and Thompson, R., 1990: A stable chemical remanence in Holocene sediments. *Journal of Geophysical Research 95(B4)*, 4471– 4479.

Snowball, I.F., 1994: Bacterial magnetite and the magnetic properties of sediments in a Swedish lake. *Earth and Planetary Science Letters 126 (1–3)*, 129-142.

Snowball, I.F., 1996: Holocene environmental change in the Abisko region of northern Sweden recorded by the mineral magnetic stratigraphy of lake sediments. *GFF 118(1)*, 9-17.

Stroeven, A. P., Hättestrand, C., Kleman, J., Heyman, J., Fabel, D., Fredin, O., Goodfellow, B. W., Harbor, J. M., Jansen, J. D., Olsen, L., Caffee, M., Fink, D., Lundqvist, J., Rosqvist, G. C., Strömberg, B. & Jans-

son, K. N., 2016: Deglaciation of Scandinavia. *Quaternary Science Reviews 147*, 91–121.

Talbot, M.R. 2001: Nitrogen isotopes in palaeolimnology. *In* W.M., Last and J.P., Smol (eds.): *Tracking Environmental Change Using Lake Sediments: Physical and Chemical Techniques,* 401-439. Developments in Paleoenvironmental Research 2, Kluwer Academic Publishers, Dordrecht.

Thompson, R., Battarbee, R.W., O'Sullivan, P.E. & Oldfield F., 1975: Magnetic Susceptibility of Lake Sediments. *Limnology and Oceanography 20(5)*, 687-698.

Unkel I., Fernandez M., Björck S., Ljung K. & Wohlfarth B., 2008: Records of environmental changes during the Holocene from Isla de los Estados (54.4°S), southeastern Tierra del Fuego. *Global Planetary Change 74*, 99–113

Yu, S., Berglund, B., Sandgren, P. & Lambeck, K., 2007: Evidence for a rapid sea-level rise 7600 yr ago. *Geology 35(10)*, 891-894.

8 Appendices

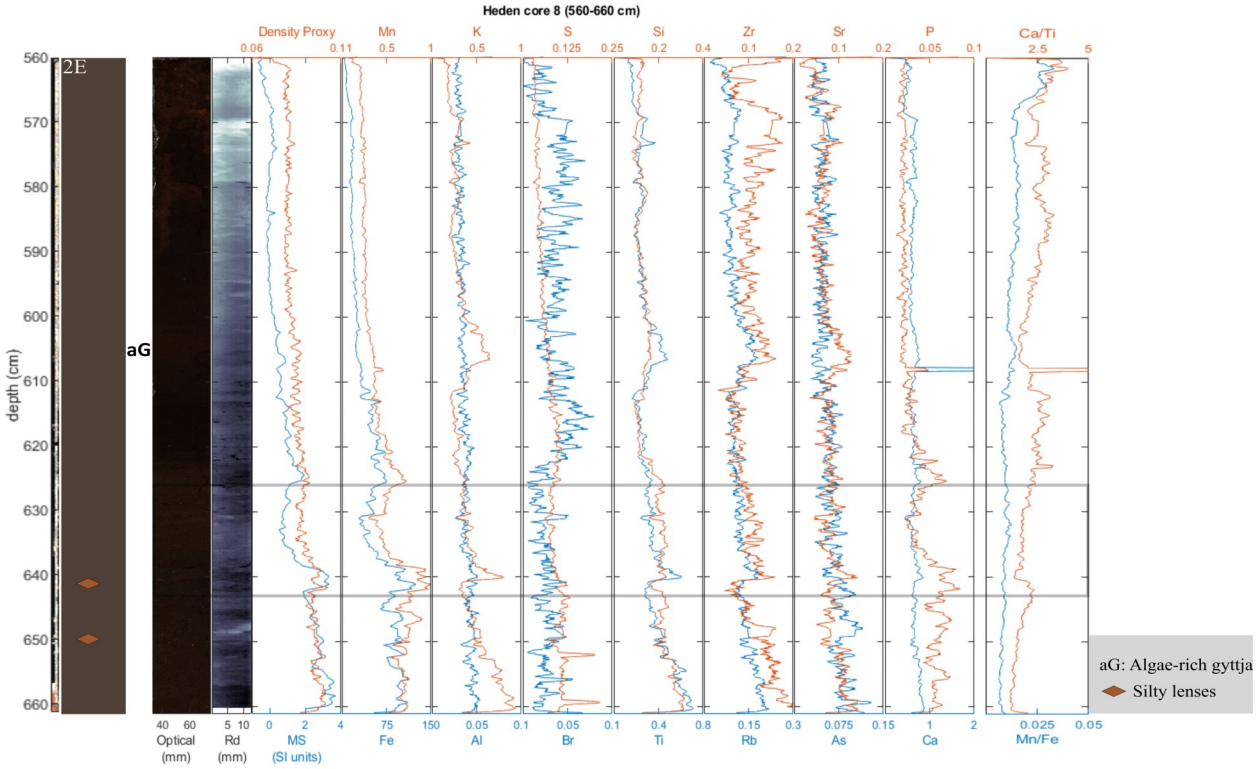

Appendix 1. Overview of core 8 (560 – 660 cm) from Heden. From left to right, the log of lithology with assigned units. The optical and radiographic (RD) image, density, magnetic susceptibility (MS), relative concentrations of typical elements for lake surveying, Ca/Ti and Mn/Fe proxies. The box indicates a zone of peculiar values.

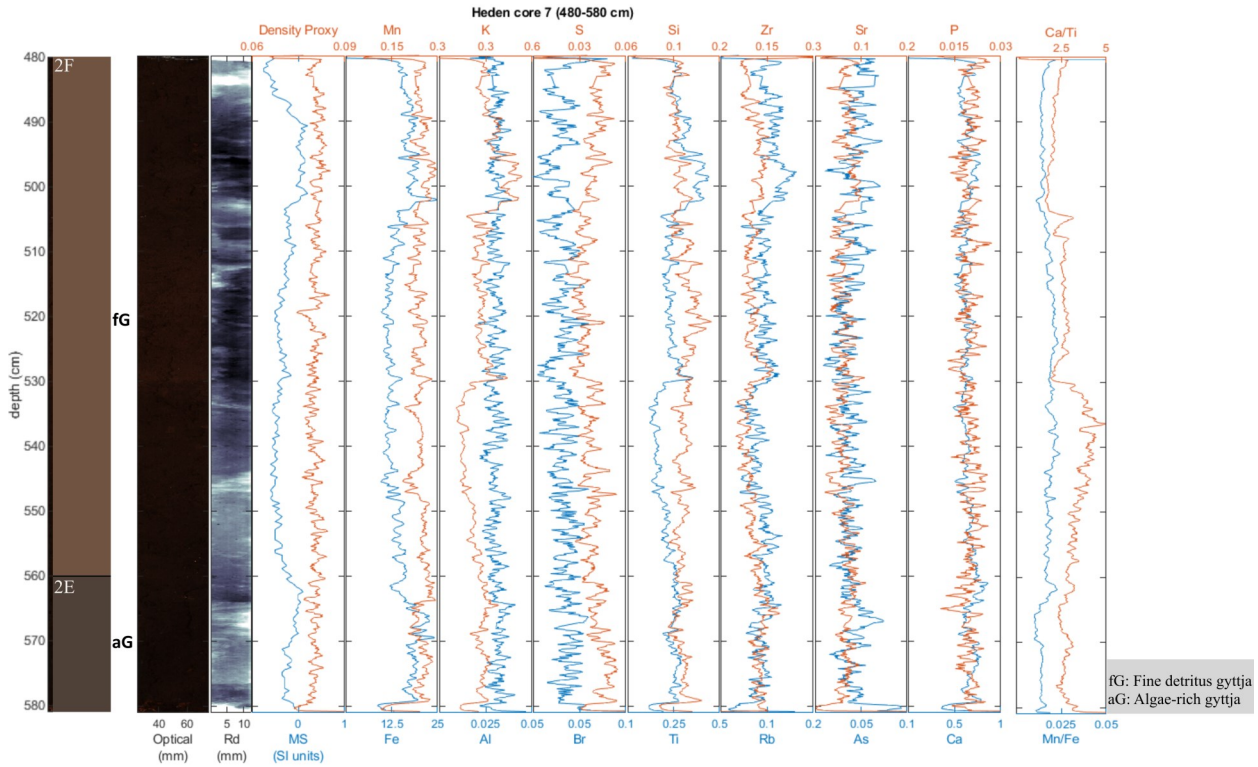

Appendix 2. Overview of core 7 (480 – 580 cm) from Heden. From left to right, the log of lithology with assigned units, and radiocarbon samples. The optical and radiographic (RD) image, density, magnetic susceptibility (MS), relative concentrations of typical elements for lake surveying, Ca/Ti and Mn/Fe proxies.

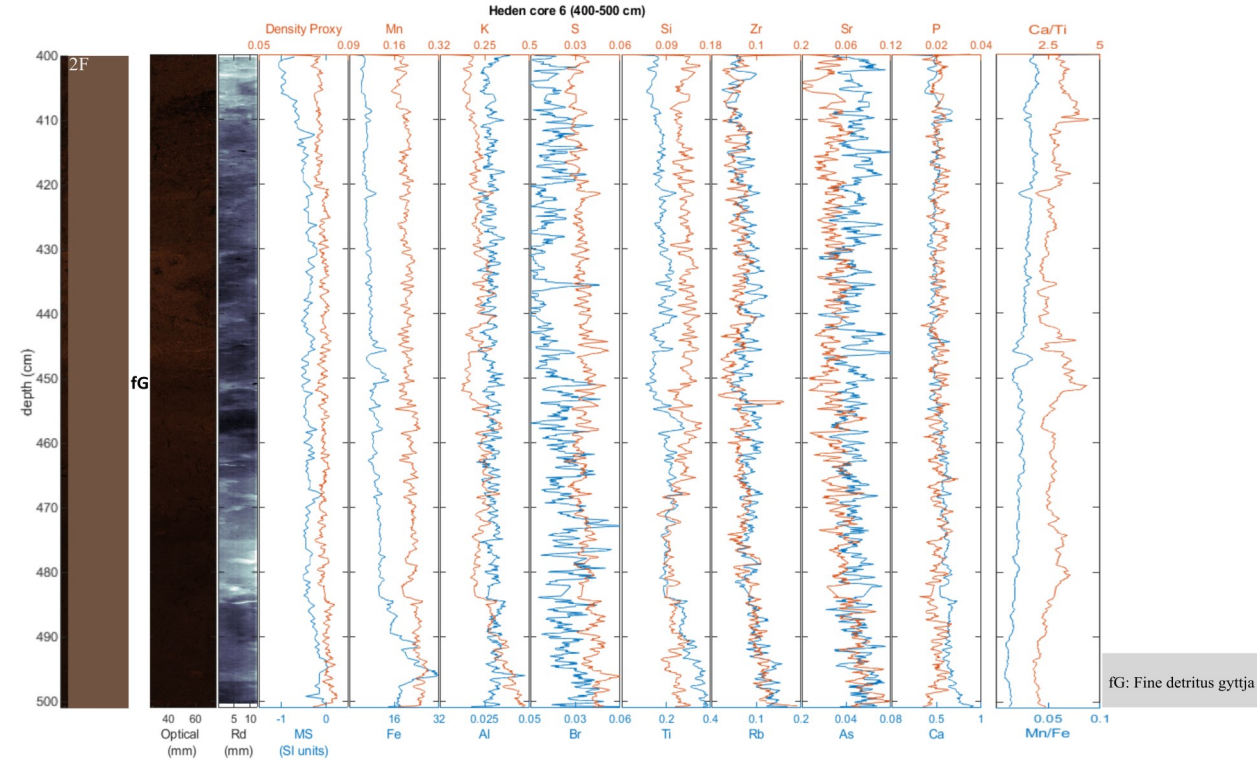

Appendix 3. Overview of core 6 (400 – 500 cm) from Heden. From left to right, the log of lithology with assigned units, the optical and radiographic (RD) image, density, magnetic susceptibility (MS), relative concentrations of typical elements for lake surveying, Ca/Ti and Mn/Fe proxies.

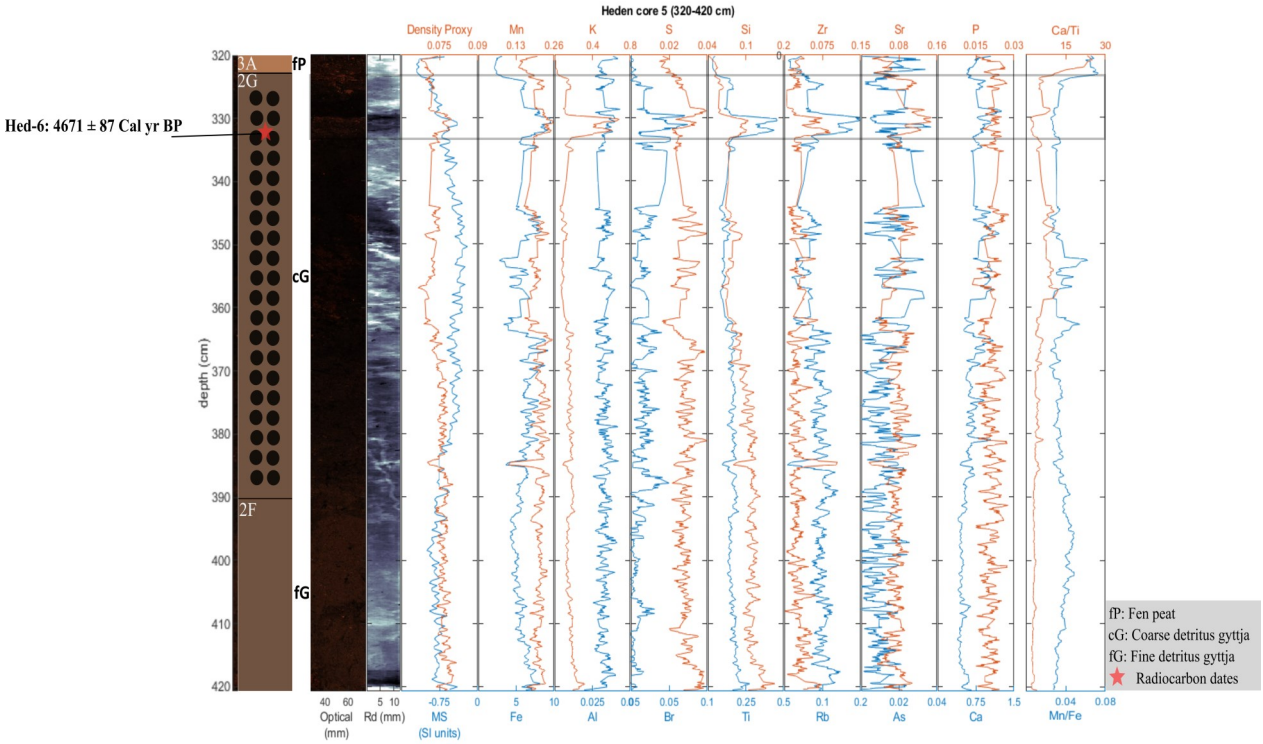

Appendix 4. Overview of core 5 (320 – 420 cm) from Heden. From left to right, the log of lithology with assigned units, and radiocarbon samples. The optical and radiographic (RD) image, density, magnetic susceptibility (MS), relative concentrations of typical elements for lake surveying, Ca/Ti and Mn/Fe proxies. The box indicates a zone of peculiar values.

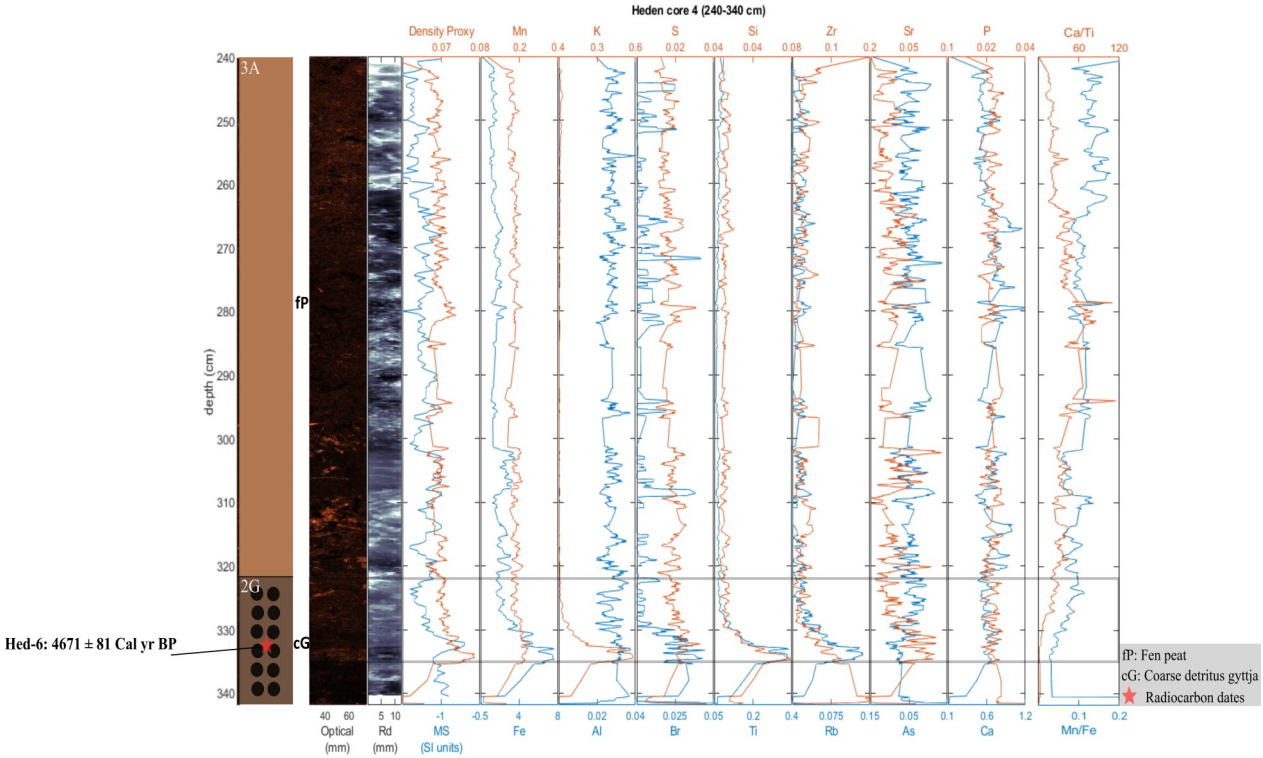

Appendix 5. Overview of core 4 (240 – 340 cm) from Heden. From left to right, the log of lithology with assigned units, and radiocarbon samples. The optical and radiographic (RD) image, density, magnetic susceptibility (MS), relative concentrations of typical elements for lake surveying, Ca/Ti and Mn/Fe proxies. The box indicates a zone of peculiar values.

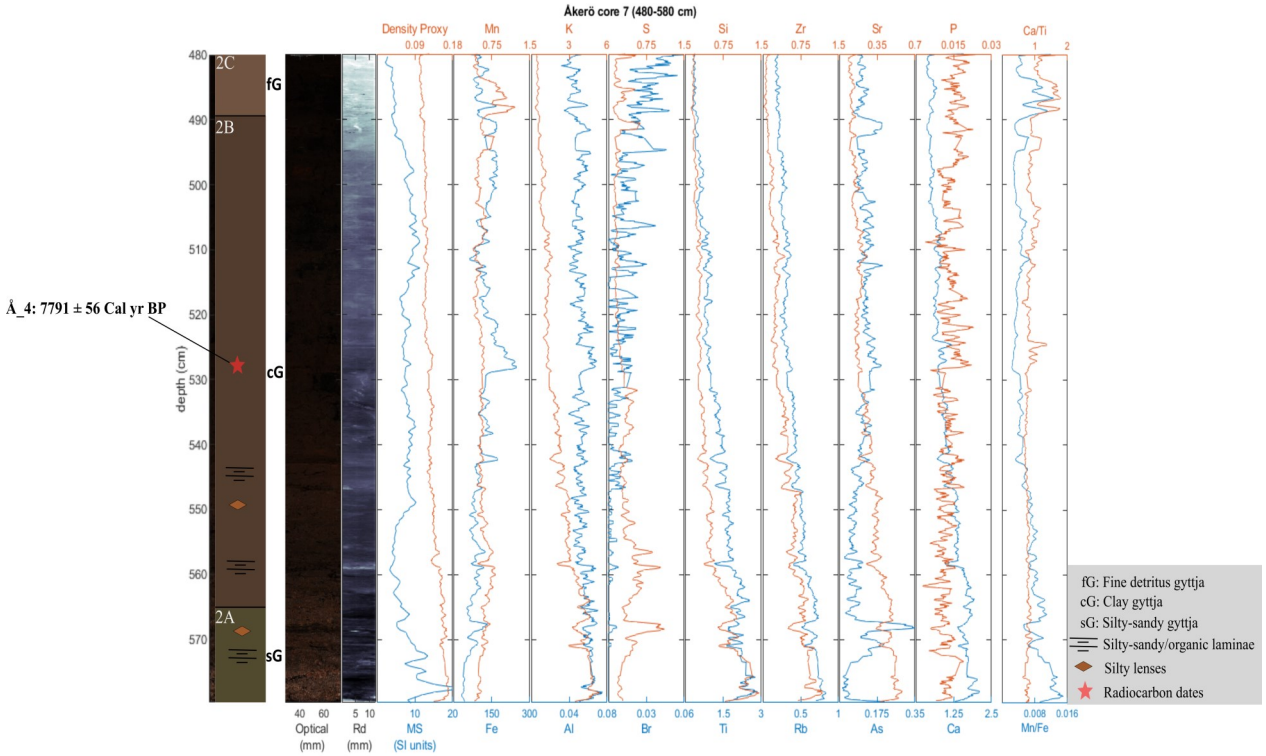

Appendix 6. Overview of core 7 (480 – 580 cm) from Åkerö. From left to right, the log of lithology with assigned units, and radiocarbon samples. The optical and radiographic (RD) image, density, magnetic susceptibility (MS), relative concentrations of typical elements for lake surveying, Ca/Ti and Mn/Fe proxies.

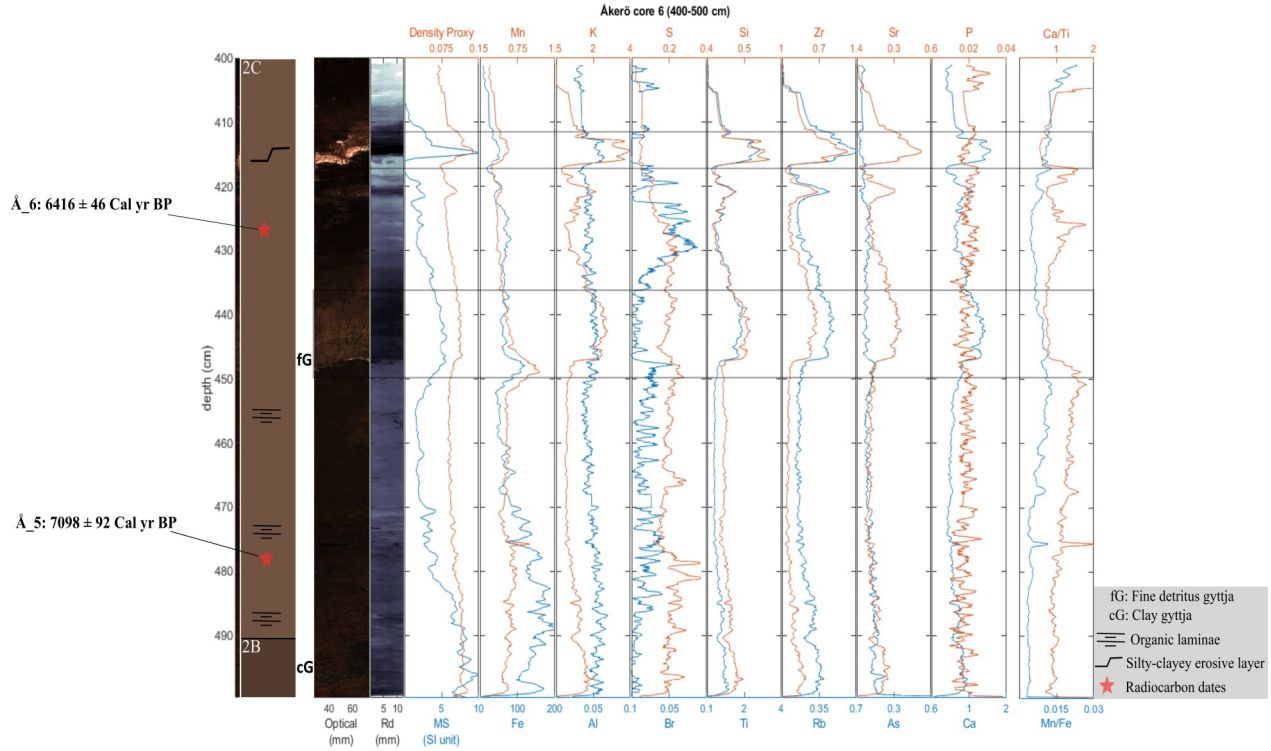

Appendix 7. Overview of core 6 (400 – 500 cm) from Åkerö. From left to right, the log of lithology with assigned units, and radiocarbon samples. The optical and radiographic (RD) image, density, magnetic susceptibility (MS), relative concentrations of typical elements for lake surveying, Ca/Ti and Mn/Fe proxies. The boxes indicate zones of peculiar values.

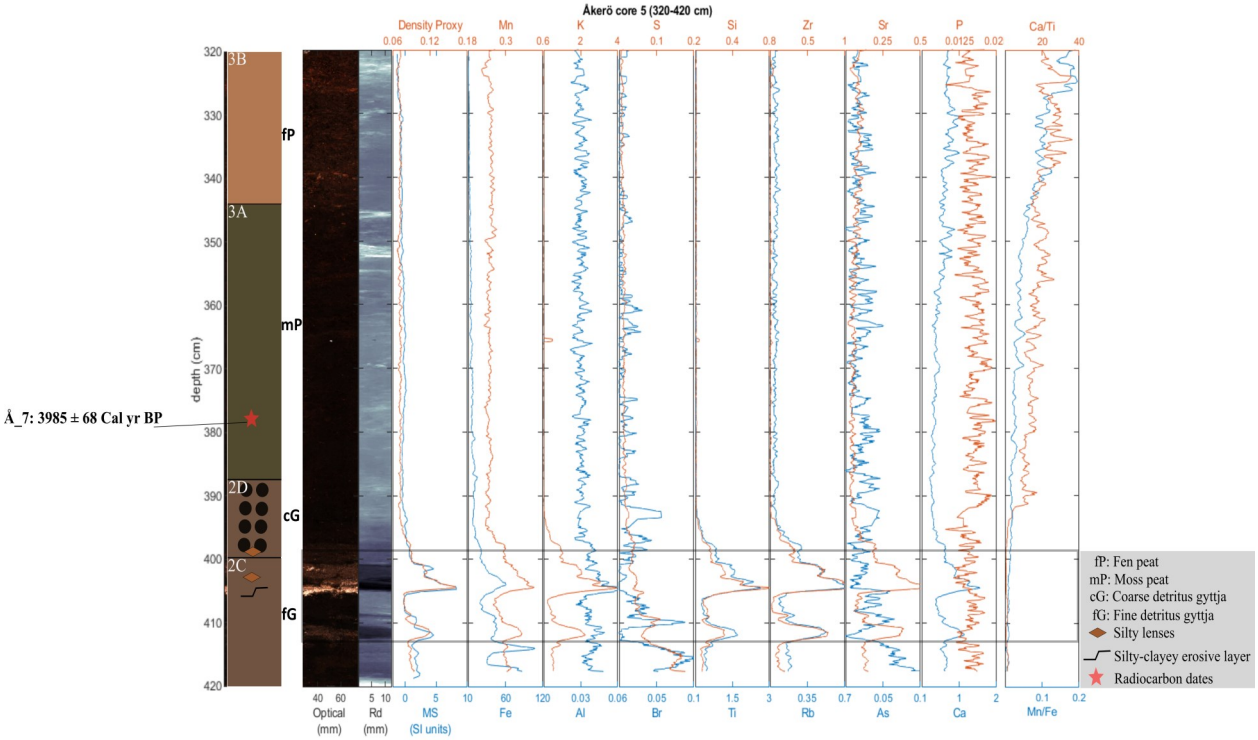

Appendix 8. Overview of core 5 (320 – 420 cm) from Åkerö. From left to right, the log of lithology with assigned units, and radiocarbon samples. The optical and radiographic (RD) image, density, magnetic susceptibility (MS), relative concentrations of typical elements for lake surveying, Ca/Ti and Mn/Fe proxies. The box indicates a zone of peculiar values.

	Al	Si	P	S	Ar	K	Ca	Ti	V	Cr	Mn	Fe	Ni	Cu	Zn	Ge	As	Br	Rb	Sr	Y	Zr	Mo	La	Ce	Nd	Tm	Yb
Al	1																											
Si	**0.645**	1																										
P	0.362	0.033	1																									
S	0.292	0.141	0.228	1																								
Ar	0.078	0.095	0.048	0.057	1																							
K	**0.716**	0.92	0.159	0.178	0.11	1																						
Ca	**0.616**	**0.691**	0.269	0.356	0.073	**0.756**	1																					
Ti	**0.694**	**0.793**	0.235	0.215	0.099	**0.917**	**0.768**	1																				
V	0.255	0.18	0.084	**0.518**	0.063	0.264	0.39	0.347	1																			
Cr	0.119	-0.175	0.326	0.255	0.034	-0.022	0.137	0.102	0.311	1																		
Mn	0.408	0.167	**0.575**	0.418	0.057	0.344	0.406	0.411	0.236	0.308	1																	
Fe	**0.568**	0.212	**0.669**	0.486	0.069	0.451	**0.527**	**0.573**	0.403	**0.507**	**0.682**	1																
Ni	-0.487	-0.466	-0.348	-0.233	0.05	**-0.526**	-0.455	**-0.526**	-0.183	0.006	-0.332	-0.525	1															
Cu	-0.497	-0.43	-0.414	-0.243	-0.084	**-0.505**	-0.453	**-0.524**	-0.16	0.192	-0.373	-0.578	0.6	1														
Zn	0.437	0.362	0.278	0.253	0.053	**0.505**	**0.593**	**0.583**	0.346	0.234	0.355	**0.581**	-0.348	-0.448	1													
Ge	-0.304	-0.27	-0.246	-0.19	-0.134	-0.337	-0.281	-0.355	-0.115	0.196	-0.278	-0.384	0.417	**0.598**	-0.258	1												
As	0.251	0.010	0.357	0.341	0.031	0.123	0.221	0.19	0.174	0.216	0.333	**0.528**	-0.283	-0.352	0.334	-0.205	1											
Br	-0.104	-0.147	-0.033	0.117	0.015	-0.142	-0.057	-0.124	0.065	0.11	-0.021	0.008	0.08	0.119	-0.015	0.094	0.125	1										
Rb	**0.697**	**0.919**	0.151	0.242	0.105	**0.947**	**0.752**	**0.873**	0.299	-0.022	0.307	0.425	**-0.521**	-0.497	0.484	-0.316	0.122	-0.133	1									
Sr	**0.617**	**0.887**	0.062	0.21	0.102	**0.86**	**0.719**	**0.783**	0.277	-0.089	0.197	0.284	-0.451	-0.436	0.409	-0.261	0.054	-0.102	**0.883**	1								
Y	0.112	0.098	0.092	-0.031	0.071	0.191	0.219	0.242	0.147	0.147	0.069	0.204	-0.09	-0.104	0.24	-0.078	0.057	0.025	0.157	0.174	1							
Zr	**0.593**	**0.781**	0.148	0.168	0.109	**0.811**	**0.682**	**0.802**	0.311	-0.076	0.242	0.396	**-0.503**	**-0.559**	**0.513**	-0.356	0.148	-0.133	**0.812**	**0.764**	0.219	1						
Mo	-0.145	-0.113	-0.145	0.159	0.149	-0.171	-0.114	-0.191	0.006	-0.245	-0.117	-0.169	0.101	-0.078	-0.022	-0.077	0.051	0.05	-0.16	-0.112	-0.027	-0.057	1					
La	0.176	0.138	0.125	0.255	0.081	0.234	0.243	0.272	0.228	0.365	0.308	0.267	0.006	0.137	0.058	0.002	-0.03	0.039	0.212	0.143	0.121	0.079	-0.192	1				
Ce	0.423	**0.595**	0.012	0.155	0.117	**0.675**	**0.565**	**0.658**	0.293	0.199	0.242	0.252	-0.186	-0.03	0.267	-0.074	-0.054	-0.05	**0.633**	**0.573**	0.201	0.488	-0.231	**0.602**	1			
Nd	-0.036	-0.314	0.257	0.218	-0.002	-0.197	-0.016	-0.098	0.304	**0.603**	0.235	0.346	0.1	0.197	0.059	0.145	0.141	0.136	-0.195	-0.252	0.076	-0.232	-0.129	0.315	-0.035	1		
Tm	0.296	-0.014	0.492	0.195	-0.001	0.138	0.216	0.238	0.207	0.347	0.321	**0.655**	-0.303	**-0.52**	0.359	-0.245	0.423	0.002	0.133	0.06	0.151	0.206	-0.081	0.010	-0.071	0.265	1	
Yb	0.087	0.371	-0.272	-0.051	0.018	0.268	0.147	0.165	0.004	-0.064	-0.135	-0.269	-0.261	0.224	-0.072	0.145	-0.216	-0.045	0.27	0.288	-0.016	0.163	-0.054	0.164	0.343	-0.115	-0.335	1

Appendix 9. Correlation coefficients of the elements detected in the Heden sediment record. Numbers marked in bold show significant positive or negative correlation (more than ± 0.5).

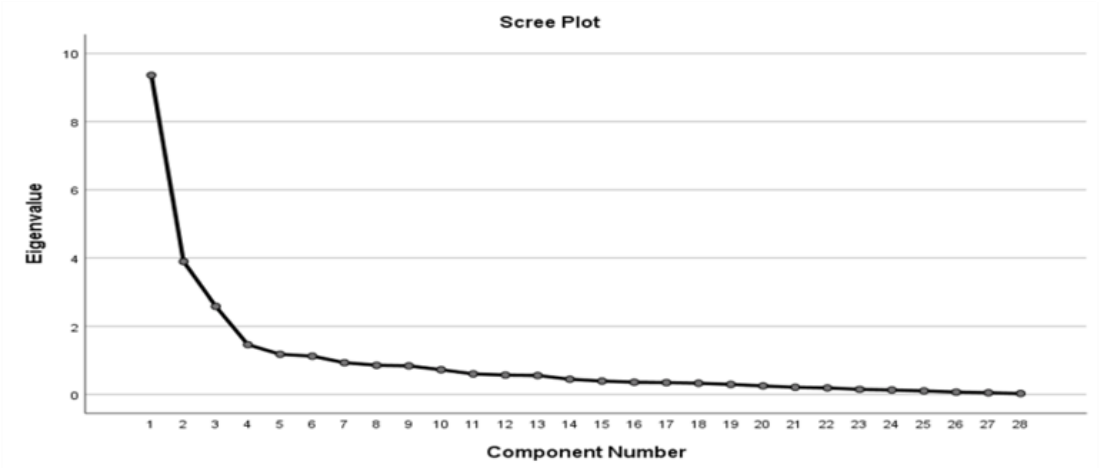

Component		1	2	3	4	5	6	7	8	9	10	11	12	13	14	15
Initial Eigenvalues	Total	9.360	3.897	2.582	1.459	1.178	1.122	0.930	0.854	0.837	0.724	0.601	0.568	0.555	0.445	0.391
	% of Variance	33.427	13.916	9.222	5.209	4.206	4.007	3.321	3.051	2.990	2.586	2.145	2.029	1.981	1.590	1.398
	Cumulative %	33.427	47.344	56.565	61.775	65.981	69.987	73.309	76.360	79.350	81.936	84.080	86.108	88.090	89.679	91.077

Appendix 10. Scree plot and PCA of the explained variance by the first fifteen components at Heden. According to the scree plot, the first three to four components are the most significant and solve most of the variance.

	Component		
	1	2	3
Al	**0.787**	0.004	-0.029
Si	**0.797**	-0.521	0.010
P	0.394	**0.602**	-0.147
S	0.394	0.385	0.120
Ar	0.122	-0.012	0.019
K	**0.908**	-0.326	0.052
Ca	**0.842**	-0.060	0.110
Ti	**0.919**	-0.157	0.076
V	0.427	0.257	0.296
Cr	0.151	**0.608**	**0.570**
Mn	**0.531**	0.480	0.055
Fe	**0.711**	**0.644**	-0.024
Zn	**0.648**	0.210	-0.065
As	0.322	**0.512**	-0.238
Br	-0.108	0.184	0.145
Rb	**0.896**	-0.329	0.048
Sr	**0.808**	-0.415	0.035
Y	0.245	0.071	0.122
Zr	**0.824**	-0.273	-0.117
Mo	-0.158	-0.032	-0.328
La	0.277	0.125	**0.683**
Ce	**0.608**	-0.284	**0.558**
Tm	0.371	**0.616**	-0.248
Ni	**-0.646**	-0.032	0.274
Cu	**-0.655**	-0.152	**0.619**
Nd	-0.043	**0.636**	0.477
Yb	0.129	**-0.537**	0.366
Ge	-0.451	-0.085	0.477

Appendix 11. PCA of the three most significant components at Heden. Strong positive or negative correlations are shown in bold.

	Al	Si	P	S	Ar	K	Ca	Ti	V	Cr	Mn	Fe	Ni	Cu	Zn	Ge	As	Br	Rb	Sr	Y	Zr	Mo	La	Ce	Nd	Tm	Yb
Al	1																											
Si	**0.927**	1																										
P	0.186	0.182	1																									
S	-0.164	-0.244	-0.086	1																								
Ar	0.099	0.097	-0.023	0.034	1																							
K	**0.913**	**0.968**	0.138	-0.105	0.114	1																						
Ca	**0.874**	**0.923**	0.168	-0.057	0.109	**0.955**	1																					
Ti	**0.755**	**0.793**	0.121	-0.027	0.087	**0.845**	**0.877**	1																				
V	0.371	0.364	0.057	-0.134	0.027	0.368	0.352	0.228	1																			
Cr	-0.428	**-0.535**	-0.094	0.185	-0.017	**-0.523**	-0.466	-0.4	0.021	1																		
Mn	0.245	0.148	-0.049	0.399	0.021	0.222	0.295	0.324	0.236	0.197	1																	
Fe	-0.366	**-0.545**	-0.202	0.397	-0.033	**-0.508**	-0.48	-0.402	-0.062	**0.58**	0.367	1																
Ni	**-0.574**	**-0.582**	0.063	-0.034	-0.121	**-0.603**	**-0.546**	-0.459	-0.346	0.256	-0.263	-0.001	1															
Cu	**-0.607**	**-0.596**	-0.035	-0.047	-0.127	**-0.611**	**-0.555**	**-0.518**	-0.204	0.41	-0.261	-0.012	**0.602**	1														
Zn	**0.519**	**0.548**	0.122	0.030	0.221	**0.596**	**0.635**	**0.581**	0.258	-0.231	0.31	-0.412	-0.208	-0.225	1													
Ge	-0.219	-0.201	0.11	-0.208	-0.228	-0.263	-0.232	-0.255	0.122	0.28	-0.129	-0.143	0.356	**0.633**	-0.088	1												
As	-0.43	**-0.531**	-0.101	0.463	0.053	-0.493	-0.461	-0.395	-0.124	0.351	0.173	**0.631**	0.122	0.049	-0.303	-0.098	1											
Br	-0.441	-0.455	0.019	-0.043	-0.134	**-0.503**	-0.48	-0.46	-0.138	0.265	-0.176	0.161	0.378	0.447	-0.278	0.321	0.203	1										
Rb	**0.882**	**0.936**	0.107	-0.075	0.112	**0.978**	**0.94**	**0.841**	0.372	-0.498	0.247	-0.462	**-0.627**	**-0.62**	**0.593**	-0.288	-0.469	**-0.518**	1									
Sr	**0.87**	**0.932**	0.127	-0.103	0.104	**0.97**	**0.948**	**0.856**	0.36	**-0.507**	0.229	**-0.51**	**-0.584**	**-0.589**	**0.606**	-0.265	-0.497	**-0.507**	**0.98**	1								
Y	-0.288	-0.356	-0.118	0.377	0.035	-0.267	-0.203	-0.124	-0.002	0.312	0.287	0.385	0.12	0.08	-0.084	-0.085	0.336	0.111	-0.229	-0.22	1							
Zr	**0.723**	**0.783**	0.156	-0.098	0.08	**0.817**	**0.847**	**0.879**	0.195	-0.443	0.216	-0.462	-0.404	**-0.512**	**0.551**	-0.252	-0.432	-0.456	**0.818**	**0.845**	-0.128	1						
Mo	0.298	0.364	0.206	-0.017	0.078	0.348	0.333	0.278	-0.104	-0.489	-0.205	-0.466	-0.029	-0.312	0.209	-0.241	-0.256	-0.233	0.295	0.312	-0.231	0.343	1					
La	-0.429	**-0.534**	-0.204	0.193	0.032	**-0.505**	-0.479	-0.409	0.216	0.567	0.242	**0.68**	0.001	0.212	-0.321	0.131	0.476	0.201	-0.461	-0.49	0.362	-0.489	-0.547	1				
Ce	**0.629**	**0.645**	-0.010	0.048	0.136	**0.718**	**0.709**	**0.662**	**0.556**	-0.177	0.373	-0.198	**-0.601**	-0.384	0.483	-0.108	-0.256	-0.403	**0.733**	**0.719**	-0.013	0.569	-0.022	0.124	1			
Nd	**-0.696**	**-0.812**	-0.172	0.186	-0.058	**-0.818**	**-0.781**	**-0.707**	-0.059	**0.698**	0.099	**0.766**	0.327	0.471	**-0.515**	0.246	**0.564**	0.418	**-0.785**	**-0.807**	0.363	-0.743	-0.562	0.786	-0.382	1		
Tm	-0.486	**-0.623**	-0.081	0.204	-0.069	**-0.619**	**-0.586**	**-0.501**	-0.073	**0.559**	0.227	**0.731**	0.268	0.112	-0.426	0.053	**0.501**	0.291	**-0.604**	**-0.617**	0.392	-0.506	-0.379	0.58	-0.362	0.718	1	
Yb	**0.775**	**0.866**	0.136	-0.207	0.084	**0.866**	**0.83**	**0.727**	0.245	-0.498	0.051	**-0.626**	**-0.572**	-0.372	**0.525**	-0.103	**-0.562**	-0.408	**0.844**	**0.852**	-0.335	0.727	0.321	-0.569	0.577	-0.786	-0.665	1

Appendix 12. Correlation coefficients of the elements detected in the Åkerö sediment record. Numbers marked in bold show significant positive or negative correlation (more than ± 0.5).

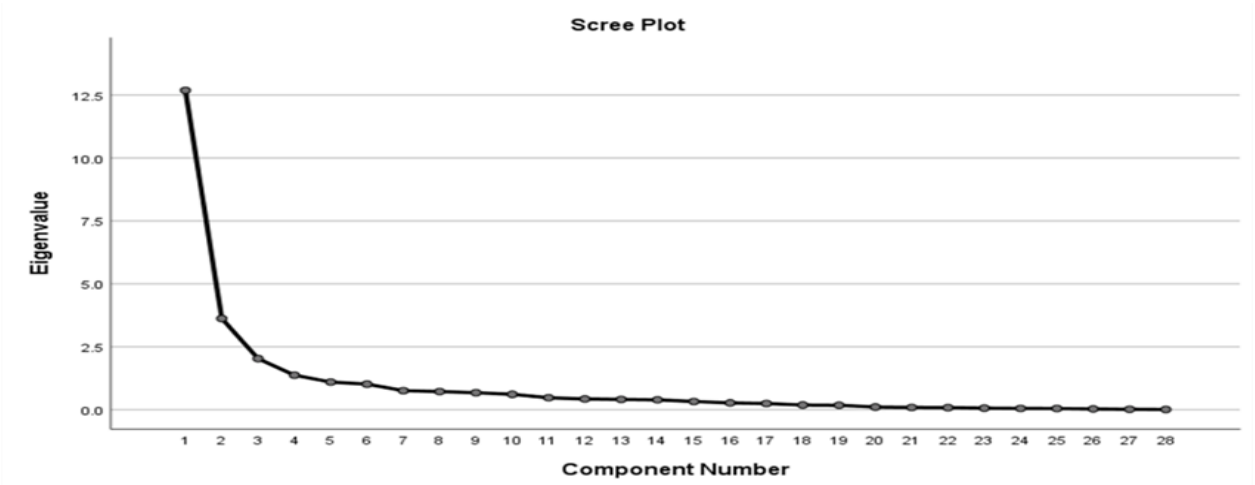

Component		1	2	3	4	5	6	7	8	9	10	11	12	13	14	15
Initial Eigenvalues	Total	12.682	3.622	2.030	1.372	1.099	1.017	0.757	0.720	0.675	0.611	0.476	0.429	0.410	0.393	0.326
	% of Variance	45.294	12.937	7.250	4.899	3.924	3.632	2.703	2.572	2.411	2.181	1.700	1.530	1.464	1.403	1.165
	Cumulative %	45.294	58.230	65.480	70.379	74.303	77.935	80.638	83.210	85.621	87.802	89.502	91.033	92.497	93.900	95.065

Appendix 13. Scree plot and PCA of the explained variance by the first fifteen components at Åkerö. According to the scree plot, the first three components are the most significant and solve most of the variance.

	Component		
	1	2	3
Al	**0.886**	0.158	0.075
Si	**0.961**	0.023	0.087
P	0.167	-0.199	0.081
S	-0.169	0.491	-0.382
Ar	0.123	0.149	-0.180
K	**0.976**	0.122	0.043
Ca	**0.948**	0.158	0.064
Ti	**0.860**	0.193	0.008
V	0.312	0.374	**0.549**
Cr	**-0.605**	0.358	0.328
Mn	0.144	**0.739**	0.060
Fe	**-0.612**	0.654	-0.153
Ni	**-0.571**	-0.459	0.031
Cu	**-0.593**	-0.384	0.457
Zn	**0.624**	0.108	0.144
Ge	-0.273	-0.302	**0.734**
As	**-0.559**	0.430	-0.303
Br	**-0.531**	-0.211	0.224
Rb	**0.959**	0.177	0.039
Sr	**0.965**	0.133	0.054
Y	-0.323	0.463	-0.089
Zr	**0.855**	0.081	-0.035
Mo	0.432	-0.388	-0.464
La	**-0.587**	**0.591**	0.284
Ce	**0.663**	0.491	0.343
Nd	**-0.885**	0.321	0.171
Tm	**-0.693**	0.401	-0.058
Yb	**0.892**	-0.094	0.136

Appendix 14. PCA of the three most significant components in Åkerö. Strong positive or negative correlations are shown in bold.

Tidigare skrifter i serien ”Examensarbeten i Geologi vid Lunds universitet”:

545. Adeen, Lina, 2018: Hur lämpliga är de geofysiska metoderna resistivitet och IP för kartläggning av PFOS? (15 hp)
546. Nilsson Brunlid, Anette, 2018: Impact of southern Baltic sea-level changes on landscape development in the Verkeån River valley at Haväng, southern Sweden, during the early and mid Holocene. (45 hp)
547. Perälä, Jesper, 2018: Dynamic Recrystallization in the Sveconorwegian Frontal Wedge, Småland, southern Sweden. (45 hp)
548. Artursson, Christopher, 2018: Stratigraphy, sedimentology and geophysical assessment of the early Silurian Halla and Klinteberg formations, Altajme core, Gotland, Sweden. (45 hp)
549. Kempengren, Henrik, 2018: Att välja den mest hållbara efterbehandlingsmetoden vid sanering: Applicering av beslutsstödsverktyget SAMLA. (45 hp)
550. Andreasson, Dagnija, 2018: Assessment of using liquidity index for the approximation of undrained shear strength of clay tills in Scania. (45 hp)
551. Ahrenstedt, Viktor, 2018: The Neoproterozoic Visingsö Group of southern Sweden: Lithology, sequence stratigraphy and provenance of the Middle Formation. (45 hp)
552. Berglund, Marie, 2018: Basaltkuppen - ett spel om mineralogi och petrologi. (15 hp)
553. Hernnäs, Tove, 2018: Garnet amphibolite in the internal Eastern Segment, Sveconorwegian Province: monitors of metamorphic recrystallization at high temperature and pressure during Sveconorwegian orogeny. (45 hp)
554. Halling, Jenny, 2019: Characterization of black rust in reinforced concrete structures: analyses of field samples from southern Sweden. (45 hp)
555. Stevic, Marijana, 2019: Stratigraphy and dating of a lake sediment record from Lyngsjön, eastern Scania - human impact and aeolian sand deposition during the last millennium. (45 hp)
556. Rabanser, Monika, 2019: Processes of Lateral Moraine Formation at a Debris-covered Glacier, Suldenferner (Vedretta di Solda), Italy. (45 hp)
557. Nilsson, Hanna, 2019: Records of environmental change and sedimentation processes over the last century in a Baltic coastal inlet. (45 hp)
558. Ingered, Mimmi, 2019: Zircon U-Pb constraints on the timing of Sveconorwegian migmatite formation in the Western and Median Segments of the Idefjorden terrane, SW Sweden. (45 hp)
559. Hjorth, Ingeborg, 2019: Paleomagnetisk undersökning av vulkanen Rangitoto, Nya Zeeland, för att bestämma dess utbrottshistoria. (15 hp)
560. Westberg, Märta, 2019: Enigmatic worm-like fossils from the Silurian Waukesha Lagerstätte, Wisconsin, USA. (15 hp)
561. Björn, Julia, 2019: Undersökning av påverkan på hydraulisk konduktivitet i förorenat område efter in situ-saneringsförsök. (15 hp)
562. Faraj, Haider, 2019: Tolkning av georadarprofiler över grundvattenmagasinet Verveln - Gullringen i Kalmar län. (15 hp)
563. Bjermo, Tim, 2019: Eoliska avlagringar och vindriktningar under holocen i och kring Store Mosse, södra Sverige. (15 hp)
564. Langkjaer, Henrik, 2019: Analys av Östergötlands kommande grundvattenresurser ur ett klimtperspektiv - med fokus på förstärkt grundvattenbildning. (15 hp)
565. Johansson, Marcus, 2019: Hur öppet var landskapet i södra Sverige under Atlantisk tid? (15 hp)
566. Molin, Emmy, 2019: Litologi, sedimentologi och kolisotopstratigrafi över krita–paleogen-gränsintervallet i borrningen Limhamn-2018. (15 hp)
567. Schroeder, Mimmi, 2019: The history of European hemp cultivation. (15 hp)
568. Damber, Maja, 2019: Granens invandring i sydvästa Sverige, belyst genom pollenanalys från Skottenesjön. (15 hp)
569. Lundgren Sassner, Lykke, 2019: Strandmorfologi, stranderosion och stranddeposition, med en fallstudie på Tylösand sandstrand, Halland. (15 hp)
570. Greiff, Johannes, 2019: Mesozoiska konglomerat och Skånes tektoniska utveckling. (15 hp)
571. Persson, Eric, 2019: An Enigmatic Cerapodian Dentary from the Cretaceous of southern Sweden. (15 hp)
572. Aldenius, Erik, 2019: Subsurface characterization of the Lund Sandstone – 3D model of the sandstone reservoir and evaluation of the geoenergy storage potential, SW Skåne, South Sweden. (45 hp)
573. Juliusson, Oscar, 2019: Impacts of subglacial processes on underlying bedrock. (15 hp)
574. Sartell, Anna, 2019: Metamorphic paragenesis and P-T conditions in garnet amphibolite from the Median Segment of the Idefjorden Terrane, Lilla Edet. (15 hp)
575. Végvári, Fanni, 2019: Vulkanisk inverkan på klimatet och atmorsfärcirkulationen: En litterarurstudie som jämför vulkanism

på låg respektive hög latitud. (15 hp)

576. Gustafsson, Jon, 2019: Petrology of platinum-group element mineralization in the Koillismaa intrusion, Finland. (45 hp)
577. Wahlquist, Per, 2019: Undersökning av mindre förkastningar för vattenuttag i sedimentärt berg kring Kingelstad och Tjutebro. (15 hp)
578. Gaitan Valencia, Camilo Esteban, 2019: Unravelling the timing and distribution of Paleoproterozoic dyke swarms in the eastern Kaapvaal Craton, South Africa. (45 hp)
579. Eggert, David, 2019: Using Very-Low-Frequency Electromagnetics (VLF-EM) for geophysical exploration at the Albertine Graben, Uganda - A new CAD approach for 3D data blending. (45 hp)
580. Plan, Anders, 2020: Resolving temporal links between the Högberget granite and the Wigström tungsten skarn deposit in Bergslagen (Sweden) using trace elements and U-Pb LA-ICPMS on complex zircons. (45 hp)
581. Pilser, Hannes, 2020: A geophysical survey in the Chocaya Basin in the central Valley of Cochabamba, Bolivia, using ERT and TEM. (45 hp)
582. Leopardi, Dino, 2020: Temporal and genetical constraints of the Cu-Co Vena-Dampetorp deposit, Bergslagen, Sweden. (45 hp)
583. Lagerstam Lorien, Clarence, 2020: Neck mobility versus mode of locomotion – in what way did neck length affect swimming performance among Mesozoic plesiosaurs (Reptilia, Sauropterygia)? (45 hp)
584. Davies, James, 2020: Geochronology of gneisses adjacent to the Mylonite Zone in southwestern Sweden: evidence of a tectonic window? (45 hp)
585. Foyn, Alex, 2020: Foreland evolution of Blåisen, Norway, over the course of an ablation season. (45 hp)
586. van Wees, Roos, 2020: Combining luminescence dating and sedimentary analysis to derive the landscape dynamics of the Velická Valley in the High Tatra Mountains, Slovakia. (45 hp)
587. Rettig, Lukas, 2020: Implications of a rapidly thinning ice-margin for annual moraine formation at Gornergletscher, Switzerland. (45 hp)
588. Bejarano Arias, Ingrid, 2020: Determination of depositional environment and luminescence dating of Pleistocene deposits in the Biely Váh valley, southern foothills of the Tatra Mountains, Slovakia. (45 hp)
589. Olla, Daniel, 2020: Petrografisk beskrivning av Prekambriska ortognejser i den undre delen av Särvskollan, mellersta delen av Skollenheten, Kaledonska orogenen. (15 hp)
590. Friberg, Nils, 2020: Är den sydatlantiska magnetiska anomalin ett återkommande fenomen? (15 hp)
591. Brakebusch, Linus, 2020: Klimat och väder i Nordatlanten-regionen under det senaste årtusendet. (15 hp)
592. Boestam, Max, 2020: Stränder med erosion och ackumulation längs kuststräckan Trelleborg - Abbekås under perioden 2007-2018. (15 hp)
593. Agudelo Motta, Laura Catalina, 2020: Methods for rockfall risk assessment and estimation of runout zones: A case study in Gothenburg, SW Sweden. (45 hp)
594. Johansson, Jonna, 2020: Potentiella nedslagskratrar i Sverige med fokus på Östersjön och östkusten. (15 hp)
595. Haag, Vendela, 2020: Studying magmatic systems through chemical analyses on clinopyroxene - a look into the history of the Teno ankaramites, Tenerife. (45 hp)
596. Kryffin, Isidora, 2020: Kan benceller bevaras över miljontals år? (15 hp)
597. Halvarsson, Ellinor, 2020: Sökande efter nedslagskratrar i Sverige, med fokus på avtryck i berggrunden. (15 hp)
598. Jirdén, Elin, 2020: Kustprocesser i Arktis – med en fallstudie på Prins Karls Forland, Svalbard. (15 hp)
599. Chonewicz, Julia, 2020: The Eemian Baltic Sea hydrography and paleoenvironment based on foraminiferal geochemistry. (45 hp)
600. Paradeisis-Stathis, Savvas, 2020: Holocene lake-level changes in the Siljan Lake District – Towards validation of von Post's drainage scenario. (45 hp)

LUNDS UNIVERSITET

Geologiska institutionen
Lunds universitet
Sölvegatan 12, 223 62 Lund